J. Fluid Mech. (2003), *vol.* 487, *pp.* 211–243.
DOI: 10.1017/S0022112003004725 Printed in the United Kingdom

Aeroacoustics of a tunnel-entrance hood with a rectangular window

By M. S. HOWE[1]†, M. IIDA[2], T. FUKUDA[2] AND T. MAEDA[2]

[1]Boston University, College of Engineering, 110 Cummington Street, Boston, MA 02215, USA
mshowe@bu.edu

[2]Railway Technical Research Institute, 2-8-38 Hikari-cho, Kokubunji-shi, Tokyo 185-8540, Japan
iida@rtri.or.jp

(Received 27 August 2002 and in revised form 12 February 2003)

An analytical and experimental investigation is made of the compression wave generated when a train enters a tunnel fitted with a long, uniform hood with a rectangular window. The window is situated at the junction of the hood and tunnel, which are taken to have the same uniform cross-sectional area. An understanding of the mechanics of this canonical configuration is important for the design of tunnel entrance hoods for new high-speed trains, with speeds in excess of $300\,\mathrm{km\,h^{-1}}$. The compression wave is formed in two stages: as the train nose enters the hood and as it passes the window. The elevated pressure within the hood produces a flow of air from the window in the form of a high-speed jet, whose inertia generates an additional rise in pressure that propagates into the tunnel as a localized pulse. Multiple reflections from the window and the hood portal cause the temporary trapping of wave energy within the hood (prior to its radiation into the tunnel). All of these aspects of the flow are modelled analytically and the results are found to be in good accord with new model-scale measurements and flow visualization studies reported in this paper.

1. Introduction

A compression wave is generated when a high-speed train enters a tunnel. The wave propagates ahead of the train at the speed of sound with an overall amplitude determined principally by the train speed U and the blockage $\mathscr{A}_o/\mathscr{A}$, where $\mathscr{A}_o$, $\mathscr{A}$ respectively denote the cross-sectional areas of the train and tunnel (Hara 1961; Hara *et al.* 1968; Ozawa *et al.* 1976, 1991; Ozawa & Maeda 1988*a*; Woods & Pope 1976). The pressure rise across the compression wave front is approximately equal to

$$\frac{\rho_o U^2}{(1-M^2)}\frac{\mathscr{A}_o}{\mathscr{A}}\left(1+\frac{\mathscr{A}_o}{\mathscr{A}}\right) \tag{1.1}$$

(Howe *et al.* 2000), where ρ_o is the mean air density and $M = U/c_o$ is the train Mach number (c_o being the speed of sound). Part of the compression wave energy radiates from the distant tunnel exit as a pressure pulse (the *micro-pressure wave*) whose strength is proportional to the compression wavefront steepness. The initial wave steepness just after the formation of the compression wave depends on U and $\mathscr{A}_o/\mathscr{A}$, but is also strongly influenced by the shapes of the tunnel entrance portal

† Author to whom correspondence should be addressed.

and the train nose (Gregoire *et al.* 1997; Iida *et al.* 1996; Ito 2000; Maeda *et al.* 1993; Matsuo *et al.* 1997; Noguchi *et al.* 1996; Ogawa & Fujii 1994, 1997; Peters 2000).

The micro-pressure wave can excite vibrations and 'rattles' in buildings near the tunnel exit, especially when the tunnel is long and the trains run on 'acoustically smooth' concrete slab tracks, which tend to promote nonlinear steepening of the wave front. The influence of wave steepening can be reduced by installing a tunnel entrance hood, consisting of a thin-walled tunnel extension ahead of the tunnel entrance. The initial rise time of the compression wave is greatly increased by permitting high-pressure air produced by an entering train to exhaust to the atmosphere through one or more windows in the hood wall (Ozawa, Uchida & Maeda 1978; Ozawa *et al.* 1991; Ozawa & Maeda 1988*b*). The corresponding increase in the initial wavefront thickness is often sufficient to reduce the amplitude of the micro-pressure wave to subjectively acceptable levels.

It has been usual hitherto to base hood design entirely on the results of model-scale experiments. However, this becomes progressively more impracticable as operating speeds increase, particularly at the much higher speeds ($U \sim 500\,\mathrm{km\,h^{-1}}$) envisaged for the new *Maglev* trains. Effective suppression of the micro-pressure wave will then probably require hood lengths that exceed about 200 m. In these circumstances it is advantageous to have available numerical or analytical design tools for determining the distribution of hood windows and sizes that produce a compression wave profile of minimal steepness. To do this it is necessary to formulate and solve the aeroacoustic problem of compression wave formation by the interaction of the moving train with the hood portal and its windows.

In this paper we develop an analytical representation and report experimental results for the canonical problem of compression wave formation in a hood with only one window. The wavefront thickness is typically of order R/M for an unmodified tunnel portal of semi-circular cross-section of radius R, and we consider the case of a long hood in which the distance of the window from the hood entrance is large compared to R/M. It will be shown how separate components of the compression wave are generated when the train nose enters the hood and also when it passes the window. Multiple reflections at the window and hood portal causes the temporary confinement of wave energy to the hood. The passage of the train nose past the window creates a high-speed jet flow out of the window, and the aerodynamic sound produced by this jet radiates into the tunnel as a low-frequency pulse that contributes significantly to the compression wave profile.

The aeroacoustic theory of compression wave generation is formulated in § 2. Formulae are derived in § 3 for the pressure attributable to the irrotational displacement of air by the moving train. These are applied in § 4 to model-scale experiments described in § 5 using a train with an elliptic nose profile. The experimental observations of the jet flow from the window are used in § 4 to develop an analytical representation of the pressure pulse generated by the jet. The derivation of a tunnel-hood Green's function used in the main text is given in the Appendix.

2. The compression wave equation

Consider a tunnel of uniform cross-section fitted with a cylindrical extension of the same cross-sectional area (the 'hood'), containing a rectangular 'window'. Our analysis will be applicable to any tunnel having these general characteristics, but for comparison with the model-scale experiments described in § 5 it is convenient to frame the discussion in terms of the idealized geometry of figure 1. The tunnel and

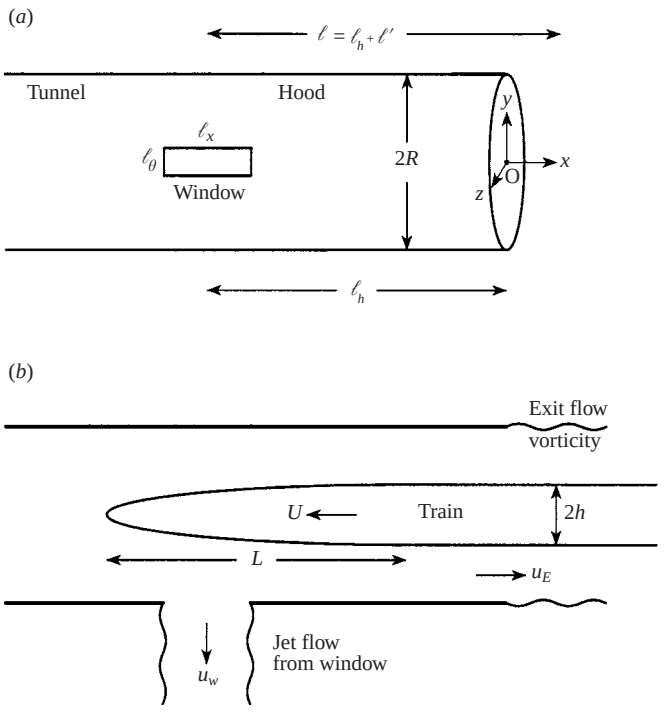

FIGURE 1. (*a*) Schematic of the circular cylindrical tunnel and hood of radius R. The hood extends from the window to the entrance plane of the cylinder; the window is rectangular with dimensions $\ell_x \times \ell_\theta$, and its geometric centre is at $x = -\ell_h,\ y = 0,\ z = R$; ℓ' is the end-correction discussed in § 3.2. (*b*) Illustration of the case of an axisymmetric train entering at speed U along the centreline of the tunnel; the exit flows from the hood portal and window are produced by the air displaced by the advancing train.

hood consist of a uniform, rigid, thin-walled circular cylindrical duct of radius R and cross-sectional area $\mathscr{A} = \pi R^2$. Coordinate axes $\boldsymbol{x} = (x, y, z)$ are taken with the origin O on the cylinder axis in the entrance plane; the x-axis is coaxial with the cylinder and is directed out of the tunnel. The window is curvilinear rectangular of length ℓ_x parallel to the cylinder axis, and with azimuthal length ℓ_θ, with the centroid of the window at $x = -\ell_h,\ y = 0,\ z = R$. The 'hood' will refer to the section of the cylinder $-\ell_h < x < 0$ between the window and the open end.

An axisymmetric train enters the hood and tunnel from $x > 0$ and travels in the negative x-direction at constant speed U. Attention will be confined to the simplest case in which the axes of the train and tunnel are coincident. It is required to determine the compression wave radiated into the tunnel ahead of the train, generated during the passage of the train nose into the hood and past the window. In a long tunnel the initial wavefront profile does not depend on the length of the tunnel, which is therefore assumed to extend to $x = -\infty$. Similarly, for the purpose of calculating this wave the length of the train may be assumed to greatly exceed the 'nose length' L indicated in the figure, beyond which the circular cross-section of the train is taken to be uniform with radius h and area $\mathscr{A}_o = \pi h^2$.

Let $\bar{p},\ \rho,\ c$ respectively denote the air pressure, density and sound speed, which are functions of position $\boldsymbol{x}$ and time t, and let $p_o,\ \rho_o,\ c_o$ be the corresponding undisturbed values. The Reynolds and Nusselt numbers based on tunnel radius R

are both typically of order 10^7 at full scale and 10^5 at model scale, so that it is permissible to neglect frictional and thermal losses during the brief interval in which the compression wave is formed (Howe 1998*a*; Howe *et al.* 2000). The initial air motion induced by the train may therefore be regarded as adiabatic, and in particular the formation of the compression wave can be calculated from the acoustic analogy equation (Howe 1998*a*)

$$\left(\frac{\mathrm{D}}{\mathrm{D}t}\left(\frac{1}{c^2}\frac{\mathrm{D}}{\mathrm{D}t}\right)-\frac{1}{\rho}\nabla\cdot(\rho\nabla)\right)B=\frac{1}{\rho}\mathrm{div}(\rho\boldsymbol{\omega}\wedge\boldsymbol{v}), \tag{2.1}$$

where $\boldsymbol{v}(\boldsymbol{x},t)$ is the velocity of the air, $\boldsymbol{\omega}=\mathrm{curl}\,\boldsymbol{v}$ is the vorticity, and $B=\int \mathrm{d}\bar{p}/\rho(\bar{p})+\frac{1}{2}v^2$ is the total enthalpy. In the region far ahead of the train occupied by the propagating wavefront, the air is linearly perturbed from its undisturbed state, and

$$B\approx\frac{p}{\rho_o},\quad \text{where}\quad p=\bar{p}-p_o. \tag{2.2}$$

The left-hand side of equation (2.1) can be replaced by the free-space acoustic wave operator if the small effects of nonlinearity on the propagation of the compression wave are ignored; this is permissible provided that only the initial form of the wave is being calculated, so that the cumulative effects of nonlinear steepening are negligible. Similarly, when the Mach number M is small the influence of compressibility in the vortex source term on the right of (2.1) can be ignored, which may therefore be replaced by $\mathrm{div}(\boldsymbol{\omega}\wedge\boldsymbol{v})$. Finally, the moving train can be represented by a distribution of monopole and dipole sources that account for the displacement of air by the train, and for the excess pressure drag on the train. It was shown by Howe *et al.* (2000) that, when the blockage $\mathscr{A}_o/\mathscr{A}\leqslant 0.2$ (the case in most applications), these distributions can be replaced by a slender-body approximation in which the monopoles and dipoles are concentrated along the axis of the train. When all of these modifications are introduced into (2.1) the equation reduces to

$$\left(\frac{1}{c_o^2}\frac{\partial^2}{\partial t^2}-\nabla^2\right)B=\frac{U}{(1-M^2)}\left(1+\frac{\mathscr{A}_o}{\mathscr{A}}\right)\frac{\partial}{\partial t}\left(\frac{\partial\mathscr{A}_{\mathrm{T}}}{\partial x}(x+Ut)\delta(y)\delta(z)\right)+\mathrm{div}(\boldsymbol{\omega}\wedge\boldsymbol{v}). \tag{2.3}$$

The first term on the right-hand side is the slender-body approximation representing the effect of the moving train. The function $\mathscr{A}_{\mathrm{T}}(s)$ is the cross-sectional area of the train at distance s from the front of the nose, which is assumed to cross the entrance plane of the hood at time $t=0$; the effective source strength is determined by the rate of change of the train cross-section, which is zero except in the nose region. The factor $1/(1-M^2)$ accounts for the Döppler amplification of the sound generated by monopole and dipole sources that occurs when they convect at speed U into a tunnel (Howe 1998*a*), and provides a small correction that is sufficient to extend the range of validity of the low-Mach-number compression wave predicted by the first source in (2.3) to $M\leqslant 0.4$ (Howe *et al.* 2000). A corresponding source distribution at the tail of a long train can be ignored for the purpose of calculating the compression wave formation.

The vorticity is non-zero principally within the shear layers formed on the moving train and in the exit flows from the hood portal and from the window. These exit flows are produced by the displacement of air by the train. When $\mathscr{A}_o/\mathscr{A}$ is small continuity implies that the velocity of the exit flow from the hood $u_{\mathrm{E}}\sim U\mathscr{A}_o/\mathscr{A}$ (see figure 1*b*), and therefore that the characteristic Mach number u_{E}/c_o is much smaller

than the train Mach number M. But the velocity u_w of the flow from the window will be shown below to be comparable to U (of order $U(2\mathscr{A}_o/\mathscr{A})^{1/2} \sim 0.65U$), so that the window jet must be expected to make a substantial contribution to the compression wave. Observation indicates that the size and extent of the shear flow over the train progressively increases with increasing distance of the train nose into the tunnel, and that it ultimately separates and forms a turbulent wake that fills much of the tunnel cross-section to the rear of the train nose (thus, for a 400 m long train the wake typically fills the tunnel at a distance of about 100 m to the rear of the nose). This causes the pressure to increase slowly with distance behind the wave front. Its contribution is strongly dependent on train and tunnel geometry, and in the model-scale experiments discussed below it is important only after the tail of the train has entered the tunnel. Its effect will not, therefore, be included in the analytical modelling of the compression wave, although we shall discuss its possible contribution further in relation to the experimental measurements.

3. Solution for irrotational flow

3.1. *General solution*

Equation (2.3) will be solved by means of Green's function $G(\boldsymbol{x}, \boldsymbol{x}', t-\tau)$, determined by

$$\left(\frac{1}{c_o^2}\frac{\partial^2}{\partial t^2} - \nabla^2\right) G = \delta(\boldsymbol{x}-\boldsymbol{x}')\delta(t-\tau), \quad G = 0 \quad \text{for } t < \tau. \tag{3.1}$$

$G(\boldsymbol{x}, \boldsymbol{x}', t-\tau)$ is the causal solution of equation (3.1) and is required to satisfy

$$\frac{\partial G}{\partial x_n} = 0 \quad \text{on the interior and exterior walls of the tunnel and hood,} \tag{3.2}$$

where x_n is a local coordinate in the normal direction from the wall. In those regions of the flow where the vorticity $\boldsymbol{\omega} = \boldsymbol{0}$ we can write $\boldsymbol{v} = \nabla\phi$ where ϕ is related to the total enthalpy B by $B = -\partial\phi/\partial t$. Condition (3.2) is therefore equivalent to the usual rigid-wall boundary condition of potential theory.

In the linearly disturbed region ahead of the train the pressure perturbation can now be expressed in the form

$$p = \frac{\rho_o U}{(1-M^2)}\left(1+\frac{\mathscr{A}_o}{\mathscr{A}}\right)\frac{\partial}{\partial t}\int_{-\infty}^{\infty}\frac{\partial \mathscr{A}_{\mathrm{T}}}{\partial x'}(x'+U\tau)G(\boldsymbol{x}, x', 0, 0, t-\tau)\,\mathrm{d}x'\,\mathrm{d}\tau$$
$$-\rho_o\int_{-\infty}^{\infty}\mathrm{d}\tau\int(\boldsymbol{\omega}\wedge\boldsymbol{v})(\boldsymbol{x}',\tau)\cdot\frac{\partial G}{\partial \boldsymbol{x}'}(\boldsymbol{x}, \boldsymbol{x}', t-\tau)\,\mathrm{d}^3\boldsymbol{x}', \quad x \to -\infty, \tag{3.3}$$

where the volume integral in the second term is taken over those regions where the vorticity $\boldsymbol{\omega} \neq \boldsymbol{0}$. Let p_0, p_ω denote the respective contributions from the two terms on the right-hand side, i.e. set

$$p = p_0 + p_\omega, \tag{3.4}$$

where p_0 is the component of pressure attributable to the source term representing the moving train, and p_ω is that produced by the vorticity.

3.2. *Evaluation of* p_0

Green's function assumes different analytic forms in different parts of the hood and tunnel. Introduce the labelling T, W, B, H, E, and A shown in the schematic figure 2(*a*), corresponding respectively to the uniform tunnel of radius R, the section

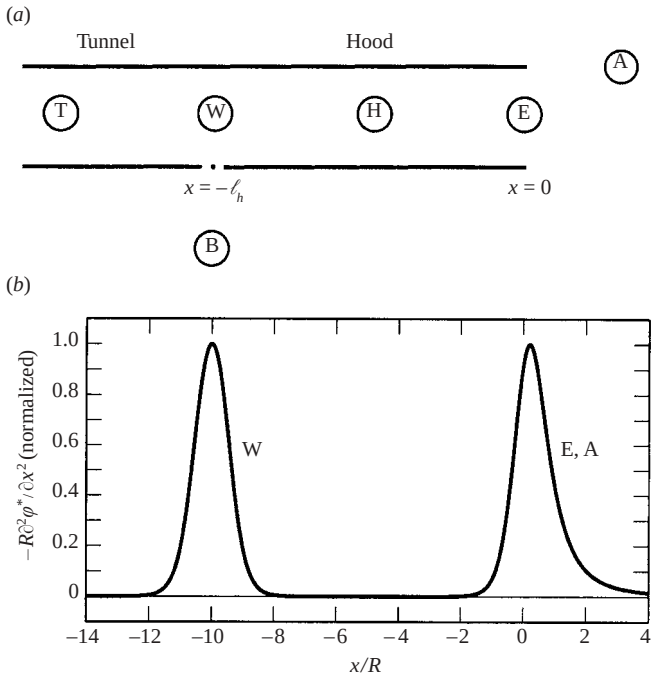

FIGURE 2. (*a*) The interior and exterior regions T, W, H, E, and A, B of the tunnel and hood used in the definition of Green's function. (*b*) Illustrating the strongly localized behaviours on the tunnel axis of $\partial^2\varphi^*_\alpha/\partial x^2$ (W) and $\partial^2\varphi^*_{\rm E}/\partial x^2$ (E, A) when $\ell_h = 10R$ for a window of dimensions $\ell_x = 0.8R$, $\ell_\theta = 0.4R$. Both plots are normalized to a maximum value of 1.

W containing the window, the region B just outside the window, the hood region H of length $\ell_h \gg R$, the hood portal E, and the neighbouring free space A outside the portal. The principal components of the compression wave are produced when the nose of the train interacts with the portal E and the window W. These interactions are conveniently isolated by first calculating the time derivative $\partial p_0/\partial t$, which is non-zero only in the vicinity of the compression wavefront, and which is conventionally referred to as the pressure gradient. We can then write (from (3.3) and (3.4), differentiating and integrating by parts)

$$\frac{\partial p_0}{\partial t} = \frac{\rho_o U^3}{(1-M^2)}\left(1+\frac{\mathscr{A}_o}{\mathscr{A}}\right)\int_{-\infty}^{\infty}\frac{\partial \mathscr{A}_{\rm T}}{\partial x'}(x'+U\tau)\frac{\partial^2 G}{\partial x'^2}(\boldsymbol{x}, x', 0, 0, t-\tau)\,{\rm d}x'\,{\rm d}\tau. \quad (3.5)$$

When this has been evaluated the pressure p_0 is readily determined by integration:

$$p_0 = \int_{-\infty}^{t}\frac{\partial p_0}{\partial t'}\,{\rm d}t'. \quad (3.6)$$

In the integrand of (3.5) $\partial^2 G/\partial x'^2$ is small except in the vicinities of the tunnel portal E and the window W. The corresponding analytical representations $G_{\rm E}$ and $G_{\rm W}$, say, of G that are respectively appropriate when the source point $\boldsymbol{x}'$ is close to E and W are found in the Appendix, where it is shown that, when the observation point $\boldsymbol{x}$ is a distance of one acoustic wavelength or more from the window within the

tunnel, we can take

$$\left.\begin{aligned} G_{\rm E}(\boldsymbol{x},\boldsymbol{x}',t-\tau) &\approx \frac{-\varphi_{\rm E}^*(\boldsymbol{x}')}{2\pi\mathscr{A}}\int_{-\infty}^{\infty}\frac{\mathscr{T}_w{\rm e}^{-{\rm i}\omega\{t-\tau+(x-\ell')/c_o\}}\,{\rm d}\omega}{1+\mathscr{R}_w{\rm e}^{2{\rm i}\kappa_o\ell}},\\ G_{\rm W}(\boldsymbol{x},\boldsymbol{x}',t-\tau) &\approx \frac{-\varphi_\alpha^*(\boldsymbol{x}')}{2\pi\mathscr{A}\ell_\alpha}\int_{-\infty}^{\infty}\frac{\mathscr{T}_w\sin(\kappa_o\ell){\rm e}^{-{\rm i}\omega\{t-\tau+(x-\ell')/c_o\}}\,{\rm d}\omega}{\kappa_o(1+\mathscr{R}_w{\rm e}^{2{\rm i}\kappa_o\ell})},\end{aligned}\right\}\quad\text{where }\kappa_o=\frac{\omega}{c_o}. \tag{3.7}$$

These representations are valid when the characteristic wavelengths of waves in the tunnel and hood are large compared to the hood radius R (i.e. the hood diameter is acoustically compact). In these circumstances the waves generated by a point source at $\boldsymbol{x}'$ in the region of the hood propagate in the tunnel towards $x=-\infty$ as plane waves functionally dependent on $t+x/c_o$. The function $\varphi_{\rm E}^*(\boldsymbol{x})$ is that solution of Laplace's equation describing irrotational flow from the mouth E of the hood, normalized such that

$$\begin{aligned}\varphi_{\rm E}^*(\boldsymbol{x}) &\sim x-\ell' \quad\text{when}\quad |\boldsymbol{x}|\gg R \quad\text{in the region H within the hood,}\\ &\sim\frac{-\mathscr{A}}{4\pi|\boldsymbol{x}|}\quad\text{when}\quad |\boldsymbol{x}|\gg R\quad\text{in the region A outside the hood,}\end{aligned} \tag{3.8}$$

where $\ell'\approx 0.61R$ is the 'end-correction' of the hood mouth (Rayleigh 1926). In (3.7) the length $\ell=\ell_h+\ell'$ (see figure 1*a*). Similarly, $\varphi_\alpha^*(\boldsymbol{x}')$ is the velocity potential representing irrotational flow out of the window for the canonical problem defined by figure 12(*b*) of the Appendix (of the ideal 'monopole' flow through the window that would be produced by motion of the pistons in figure 12(*b*) at unit speed towards each other), with the normalization

$$\begin{aligned}\varphi_\alpha^*(\boldsymbol{x}) &\sim -|x+\ell_h|-\ell_\alpha \text{ when } |x+\ell_h|\gg R \text{ in regions T and H}\\ &\sim -\frac{\mathscr{A}}{2\pi|\boldsymbol{x}|}\text{ when } |\boldsymbol{x}|\to\infty \text{ in region B outside the window.}\end{aligned} \tag{3.9}$$

The length $\ell_\alpha\equiv 2\mathscr{A}/K$, where K is the Rayleigh conductivity of the window (Rayleigh 1926), given approximately by

$$\frac{1}{K}=\frac{1}{2}\sqrt{\frac{\pi}{\mathscr{A}_w}}+\frac{\ell_w}{\mathscr{A}_w}, \tag{3.10}$$

where $\mathscr{A}_w=\ell_x\ell_\theta$ is the window area and ℓ_w is the thickness of the tunnel/hood wall.

The asymptotic formulae (3.8) imply that the second derivative $\partial^2\varphi_{\rm E}^*/\partial x^2$ is small except in the vicinity of the portal E, as indicated by the curve labelled E, A in figure 2(*b*). Similarly $\partial^2\varphi_\alpha^*/\partial x^2$ vanishes except close to the window; the W-curve in figure 2(*b*) illustrates this when the window has the dimensions $\ell_x=0.8R$, $\ell_\theta=0.4R$. The case plotted in figure 2 is for a hood of length $\ell_h=10R$; the wide separation of the curves in figure 2(*b*) shows how in this case equations (3.5), (3.7) determine two essentially distinct contributions to the pressure gradient $\partial p_0/\partial t$: the first produced when the 'centroid' of the train nose is within a distance $\sim 2R$ from the portal E and the second when it is closer than a distance R from the centre of the window. Because the functions φ_α^* and $\varphi_{\rm E}^*$ satisfy Laplace's equation, the solutions for convecting source distributions determined by the approximations (3.7) are strictly valid only for very small Mach number (Howe 1998*b*). However, it was shown by Howe *et al.* (2000) that inclusion of the factor $1/(1-M^2)$ in the representation (3.5) (which accounts for the Döppler amplification of the sound when a source is convected into a semi-infinite duct) is sufficient to preserve the validity of the theory up to $M\sim 0.4$.

The functions $\mathscr{R}_w$, $\mathscr{T}_w$ in (3.7) are respectively reflection and transmission coefficients that determine the complex amplitudes of long-wavelength plane waves in an infinitely long tunnel that would be reflected at the window and transmitted past the window when a plane wave proportional to $\mathrm{e}^{\mathrm{i}(\kappa_o x-\omega t)}$ propagates towards the window. It is shown in the Appendix that

$$\mathscr{R}_w = \frac{-1}{1-\mathrm{i}\kappa_o\ell_\alpha}, \quad \mathscr{T}_w = \frac{-\mathrm{i}\kappa_o\ell_\alpha}{1-\mathrm{i}\kappa_o\ell_\alpha}. \tag{3.11}$$

The ratio ℓ_α/c_o is a characteristic 'relaxation' time for the window. For a disturbance whose time scale exceeds ℓ_α/c_o (so that $\kappa_o\ell_\alpha \ll 1$) the window behaves as a pressure node, where total reflection occurs. At higher frequencies a disturbance propagates past the window essentially without change.

The integrations in (3.7) are conveniently performed by noting that $|\mathscr{R}_w| < 1$ for real values of ω, and by then introducing the expansion

$$\frac{1}{1+\mathscr{R}_w\mathrm{e}^{2\mathrm{i}\kappa_o\ell}} = \sum_{n=0}^{\infty}\mathscr{R}_{\mathrm{E}}^n\mathscr{R}_w^n\mathrm{e}^{2\mathrm{i}n\kappa_o\ell}, \quad \mathscr{R}_{\mathrm{E}} = -1. \tag{3.12}$$

The term of order n represents a component of the disturbance generated by the point source at $\boldsymbol{x}'$ that has been temporarily confined to the hood H by n reflections at the window with reflection coefficient $\mathscr{R}_w$ and n reflections from the open end of the hood with reflection coefficient $\mathscr{R}_{\mathrm{E}} = -1$. The causality condition of (3.1), that requires G to vanish for $t < \tau$, is satisfied because the path of integration in (3.7) passes above the singularities of the integrands in the complex ω-plane. After introducing the expansion (3.12) the integrals may then be evaluated by residues to yield

$$\begin{aligned} G_{\mathrm{E}}(\boldsymbol{x},\boldsymbol{x}',t-\tau) \;\approx\; & -\frac{\varphi_{\mathrm{E}}^*(\boldsymbol{x}')}{\mathscr{A}} \\ & \times\left\{\delta\left(t-\tau+\frac{x-\ell'}{c_o}\right)-\frac{c_o}{\ell_\alpha}\mathrm{H}\left(t-\tau+\frac{x-\ell'}{c_o}\right)\exp\left(-\frac{c_o}{\ell_\alpha}\left(t-\tau+\frac{x-\ell'}{c_o}\right)\right)\right. \\ & +\sum_{n=1}^{\infty}\frac{c_o}{\ell_\alpha}\left[\frac{1}{(n-1)!}\left(\frac{c_o}{\ell_\alpha}\right)^{n-1}\left(t-\tau+\frac{x-\ell'-2n\ell}{c_o}\right)_+^{n-1}\right. \\ & \left.\left.-\frac{1}{n!}\left(\frac{c_o}{\ell_\alpha}\right)^{n}\left(t-\tau+\frac{x-\ell'-2n\ell}{c_o}\right)_+^{n}\right]\exp\left(-\frac{c_o}{\ell_\alpha}\left(t-\tau+\frac{x-\ell'-2n\ell}{c_o}\right)\right)\right\}, \\ & x\to-\infty, \end{aligned} \tag{3.13}$$

$$\begin{aligned} G_{\mathrm{W}}(\boldsymbol{x},\boldsymbol{x}',t-\tau) \approx\; & \frac{c_o\varphi_\alpha^*(\boldsymbol{x}')}{2\mathscr{A}\ell_\alpha}\sum_{n=0}^{\infty}\frac{1}{n!}\left(\frac{c_o}{\ell_\alpha}\right)^n\left\{\left(t-\tau+\frac{x-\ell'-(2n+1)\ell}{c_o}\right)_+^n\right. \\ & \times\exp\left(-\frac{c_o}{\ell_\alpha}\left(t-\tau+\frac{x-\ell'-(2n+1)\ell}{c_o}\right)\right) \\ & -\left(t-\tau+\frac{x-\ell'-(2n-1)\ell}{c_o}\right)_+^n \\ & \left.\times\exp\left(-\frac{c_o}{\ell_\alpha}\left(t-\tau+\frac{x-\ell'-(2n-1)\ell}{c_o}\right)\right)\right\}, \quad x\to-\infty, \end{aligned} \tag{3.14}$$

where $\delta(x)$, $\mathrm{H}(x)$ respectively denote the Dirac delta-function and the Heaviside step function, and $x_+^n = \mathrm{H}(x)x^n$.

The terms in these formulae represent plane waves propagating into the tunnel (as functions of $t + x/c_o$) from the point source at $(\boldsymbol{x}', \tau)$. The component $G_{\mathrm{E}}(\boldsymbol{x}, \boldsymbol{x}', t-\tau)$ is the field radiated into the tunnel when $\boldsymbol{x}'$ is close to the entrance E of the hood. The particular case in which there is no window is recovered by taking the limit $\ell_\alpha = 2\mathscr{A}/K \to \infty$; all terms except the δ-function (which is the direct wave from the source) in the braces of (3.13) vanish in this limit, and G_{E} reduces to the corresponding approximation for a source near the entrance of a closed cylindrical tunnel (see Howe 1998*b*). The second term in the braces of (3.13) represents the (irrotational) modification of the direct wave as it propagates past the window into the tunnel. If the window is very large the pressure perturbation at the window must vanish, and the direct wave is unable to penetrate beyond it into the tunnel; in this limit the conductivity $K \to \infty$ ($\ell_\alpha \to 0$) and the second term in the braces of (3.13) tends to a δ-function that just cancels the direct wave. The interaction of the direct wave with the window produces a reflected wave that subsequently experiences multiple reflections at the open end E and at the window W, part of its energy being transmitted into the tunnel at each interaction with the window: the influence of these interactions is described by the infinite series in (3.13).

The various terms contributing to the representation (3.14) of G_{W} (the plane waves generated by the point source when $\boldsymbol{x}'$ is near W) can be interpreted similarly. In this case the direct wave from the source has the step-wave character of the Heaviside unit function.

3.3. *Pressure rise across the wave front*

The overall properties of the compression wavefront are governed by the component p_0 of the pressure. The relatively slow rise in pressure behind the wavefront observed in practice is produced by the vorticity source term on the right of (2.3), and occurs over a much longer time scale, although the net pressure rise can be substantial. The influence of the jet flow from the window is discussed in § 4, where it will be shown to generate a transient pressure pulse that makes a significant contribution to the profile of the compression wave front. Let Δp denote the pressure rise across the wavefront when the motion is entirely irrotational. We can calculate Δp from (3.6) by taking the limit $t \to \infty$ provided we ignore contributions to the train source strength $\partial\mathscr{A}_{\mathrm{T}}/\partial x$ from the tail of the train. This is equivalent to considering a train of 'semi-infinite' length, so that $\partial\mathscr{A}_{\mathrm{T}}/\partial x$ is non-zero only in the vicinity of the nose, and $\mathscr{A}_{\mathrm{T}} = \mathscr{A}_o$ to the rear of the nose.

Set

$$\Delta p = \Delta p_{\mathrm{E}} + \Delta p_{\mathrm{W}}, \tag{3.15}$$

where the terms on the right correspond respectively to the net pressure rise across the components of the compression wave produced by the interaction of the nose with the portal E and with the window W. These components are found by taking in turn $G = G_{\mathrm{E}}$, G_{W} in (3.5). Thus, setting $t = +\infty$ in (3.6) and using the first of (3.7), we find

$$\Delta p_{\mathrm{E}} = \frac{-\rho_o U^3}{2\pi\mathscr{A}(1-M^2)}\left(1+\frac{\mathscr{A}_o}{\mathscr{A}}\right) \times \int_{-\infty}^{\infty} \frac{\partial^2\varphi_{\mathrm{E}}^*}{\partial x'^2}(x',0,0)\frac{\partial\mathscr{A}_{\mathrm{T}}}{\partial x'}(x'+U\tau)\frac{\mathscr{T}_w \mathrm{e}^{-\mathrm{i}\omega\{t-\tau+(x-\ell')/c_o\}}}{1+\mathscr{R}_w \mathrm{e}^{2\mathrm{i}\kappa_o\ell}}\,\mathrm{d}\omega\,\mathrm{d}x'\,\mathrm{d}\tau\,\mathrm{d}t. \tag{3.16}$$

Now $\int_{-\infty}^{\infty} \mathrm{e}^{-\mathrm{i}\omega\{t-\tau+(x-\ell')/c_o\}}\,\mathrm{d}t = 2\pi\delta(\omega)$ and

$$\frac{\mathscr{T}_w}{1+\mathscr{R}_w \mathrm{e}^{2\mathrm{i}\kappa_o \ell}} \to \frac{\ell_\alpha}{\ell_\alpha + 2\ell} \quad \text{as } \omega \to 0,$$

so that, making the substitution $\xi = x' + U\tau$ and recalling the limiting behaviours (3.8), we find

$$\begin{aligned}\Delta p_{\mathrm{E}} &= \frac{-\rho_o U^2}{\mathscr{A}(1-M^2)}\left(1+\frac{\mathscr{A}_o}{\mathscr{A}}\right)\frac{\ell_\alpha}{\ell_\alpha+2\ell}\int_{-\infty}^{\infty}\frac{\partial^2 \varphi_{\mathrm{E}}^*}{\partial x'^2}(x',0,0)\frac{\partial \mathscr{A}_{\mathrm{T}}}{\partial \xi}(\xi)\,\mathrm{d}x'\,\mathrm{d}\xi \\ &= \frac{\rho_o U^2}{(1-M^2)}\frac{\mathscr{A}_o}{\mathscr{A}}\left(1+\frac{\mathscr{A}_o}{\mathscr{A}}\right)\frac{\ell_\alpha}{\ell_\alpha+2\ell}, \end{aligned} \tag{3.17}$$

because $\mathscr{A}_{\mathrm{T}}(\xi) = \mathscr{A}_o,\ 0$ respectively for $\xi \to \pm\infty$.

A similar calculation using G_{W} reveals that

$$\Delta p_{\mathrm{W}} = \frac{\rho_o U^2}{(1-M^2)}\frac{\mathscr{A}_o}{\mathscr{A}}\left(1+\frac{\mathscr{A}_o}{\mathscr{A}}\right)\frac{2\ell}{\ell_\alpha+2\ell}. \tag{3.18}$$

The net pressure rise (3.15) across the wavefront produced by the interaction of the train nose with the entrance portal E and the window W is therefore precisely equal to that quoted above in (1.1) for an arbitrary uniform tunnel.

3.4. *The snub-nosed train*

A particularly simple representation of the irrotational-flow compression wave can be derived for the special case of a semi-infinite 'snub-nosed' train, obtained by considering the formal limit $L \to 0$, in which the length of the train nose vanishes. In that case

$$\frac{\partial \mathscr{A}_{\mathrm{T}}}{\partial x}(x+Ut) \to \mathscr{A}_o \delta(x+Ut), \tag{3.19}$$

which permits the immediate evaluation of one of the integrations in the representation (3.5) of $\partial p_0/\partial t$. The train nose is now equivalent to a point source that crosses the entrance plane of the hood at $t = 0$. If $p_{\mathrm{SN}}(x,t)$ denotes the compression wave component $p_0(x,t)$ radiated ahead of the train in this case, then the relation

$$\frac{\partial \mathscr{A}_{\mathrm{T}}}{\partial x}(x+Ut) = \int_{-\infty}^{\infty}\frac{\partial \mathscr{A}_{\mathrm{T}}}{\partial \xi}(\xi)\,\delta(x+Ut-\xi)\,\mathrm{d}\xi$$

implies that for an arbitrary nose profile the pressure gradient $\partial p_0/\partial t$ can be cast in the form

$$\frac{\partial p_0}{\partial t} = \int_{-\infty}^{\infty}\frac{1}{\mathscr{A}_o}\frac{\partial \mathscr{A}_{\mathrm{T}}}{\partial \xi}(\xi)\frac{\partial p_{\mathrm{SN}}}{\partial t}(x, t-\xi/U)\,\mathrm{d}\xi. \tag{3.20}$$

Let

$$p_{\mathrm{SN}} = p_{\mathrm{E}} + p_{\mathrm{W}}; \tag{3.21}$$

the terms on the right respectively denote the contributions to the compression wave generated by the irrotational interactions with the hood portal and the window, determined by the corresponding components G_{E}, G_{W} of the Green's function given in (3.13) and (3.14). Then, using (3.19) and (3.13) in (3.5), we find

$$\begin{aligned}\frac{\partial p_{\mathrm{E}}}{\partial t}(x,t) = {} & \frac{-\rho_o U^3}{R(1-M^2)}\frac{\mathscr{A}_o}{\mathscr{A}}\left(1+\frac{\mathscr{A}_o}{\mathscr{A}}\right) \\ & \times\left\{\Phi''_{\mathrm{E}}\left(\frac{-U[t]}{R}\right)-\frac{(R/\ell_\alpha)}{M}\int_{\lambda_o}^{\infty}\Phi''_{\mathrm{E}}(\lambda)\exp\left(-\frac{(R/\ell_\alpha)}{M}(\lambda-\lambda_0)\right)\mathrm{d}\lambda\right. \\ & +\frac{(R/\ell_\alpha)}{M}\sum_{n=1}^{\infty}\int_{\lambda_n}^{\infty}\Phi''_{\mathrm{E}}(\lambda)\left[\frac{(R/\ell_\alpha M)^{n-1}}{(n-1)!}(\lambda-\lambda_n)^{n-1}\right. \\ & \left.\left.-\frac{(R/\ell_\alpha M)^n}{n!}(\lambda-\lambda_n)^n\right]\exp\left(-\frac{(R/\ell_\alpha)}{M}(\lambda-\lambda_n)\right)\mathrm{d}\lambda\right\}, \quad x\to-\infty, \end{aligned} \tag{3.22}$$

where the retarded time $[t]$ and λ_n are defined as follows:

$$[t]=t+\frac{x-\ell'}{c_o}, \quad \lambda_n=-\left(\frac{U[t]}{R}-\frac{2nM\ell}{R}\right), \ n\geqslant 0. \tag{3.23}$$

Φ''_{E} is the non-dimensional function defined by

$$\Phi''_{\mathrm{E}}(\lambda)=R\frac{\partial^2\varphi^*_{\mathrm{E}}}{\partial x^2}(x,0,0), \quad \text{with } \lambda=\frac{x}{R}, \tag{3.24}$$

and is determined by equations (A 18) of the Appendix. It vanishes except in the vicinity of $\lambda=x/R=0$, as indicated in figure 2(*b*).

When $\partial p_{\mathrm{E}}/\partial t$ has been evaluated from (3.22) the corresponding pressure profile generated by the snub-nosed train interacting with the portal is determined by (3.6). Figure 3(*a*) illustrates a typical prediction for the case (also discussed in § 4 in relation to our model-scale experiments) where

$$\ell_h=10R, \quad \ell_x=0.8R, \quad \ell_\theta=0.4R, \quad \ell_w=0.1R, \quad U=352\,\mathrm{km\,h^{-1}} \quad (M=0.29). \tag{3.25}$$

The length $\ell_\alpha=2\mathscr{A}/K\approx 11.81R$, where the window conductivity K is given by Rayleigh's (1926) formula (3.10). The plots of p_{E} and $\partial p_{\mathrm{E}}/\partial t$ shown in the figure are the normalized values:

$$p_{\mathrm{E}}\Big/\frac{\rho_o U^2}{(1-M^2)}\frac{\mathscr{A}_o}{\mathscr{A}}\left(1+\frac{\mathscr{A}_o}{\mathscr{A}}\right), \qquad \frac{\partial p_{\mathrm{E}}}{\partial t}\Big/\frac{\rho_o U^3}{R(1-M^2)}\frac{\mathscr{A}_o}{\mathscr{A}}\left(1+\frac{\mathscr{A}_o}{\mathscr{A}}\right). \tag{3.26}$$

In figure 3 the point source representing the nose of the train enters the hood at $U[t]/R\approx 0$. Referring to the 'pressure gradient' curve in figure 3(*a*): the large peak at $U[t]/R=0$ and the negative dip at $U[t]/R\approx 1$ are produced respectively by the first and second terms in the braces of (3.22). The first term is identical with the pressure gradient that would be generated in the absence of the window (the 'direct pulse'); it is modified by the second, integrated term which therefore determines the

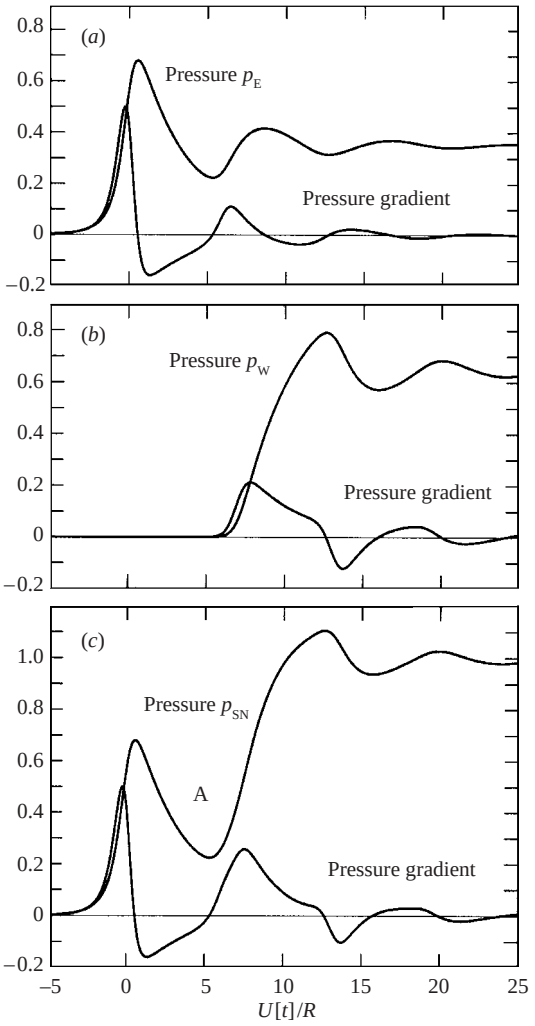

FIGURE 3. Compression wave and pressure gradient produced by a snub-nosed train when $\ell_h = 10R$, $\ell_x = 0.8R$, $\ell_\theta = 0.4R$, $\ell_w = 0.1R$, $U = 352\,\mathrm{km\,h^{-1}}$. (*a*) The pressure p_E and pressure gradient $\partial p_E/\partial t$ (normalized as in (3.26)) generated at the hood portal; (*b*) the corresponding pressure p_W and pressure gradient $\partial p_W/\partial t$ generated at the window; (*c*) the overall pressure p_{SN} and pressure gradient $\partial p_{SN}/\partial t$. The point labelled A is discussed in §4.

fraction of the 'direct pulse' transmitted past the window into the tunnel. The second positive peak in the pressure gradient occurs near $U[t]/R = 6.5$ and is produced by the first term $n = 1$ of the infinite series; it represents the wave energy transmitted into the tunnel after one reflection of the 'direct pulse' at the window and at the open end of the hood. The amplitudes of successively reflected waves (corresponding to values of $n > 1$) evidently decrease very rapidly as n increases. The characteristic width of the different pulses contributing to $\partial p_E/\partial t \sim 2R/M \approx 7R$, which is large compared to the tunnel diameter, but smaller than the hood length ℓ_h. At large times the pressure rise p_E approaches the limiting value given in (3.17); this corresponds to a non-dimensional pressure equal to 0.36.

In a similar way we find, using (3.14), the irrotational window-generated pressure gradient in the form

$$\frac{\partial p_{\mathrm{W}}}{\partial t}(x,t) = \frac{-\rho_o U^3}{R(1-M^2)}\frac{\mathscr{A}_o}{\mathscr{A}}\left(1+\frac{\mathscr{A}_o}{\mathscr{A}}\right)\frac{(R/\ell_\alpha)}{2M}\sum_{n=0}^{\infty}\frac{(R/\ell_\alpha M)^n}{n!}$$
$$\times\left\{\int_{\Lambda_{n-1/2}}^{\infty}\Phi''_{\mathrm{W}}(\lambda)\left(\lambda-\Lambda_{n-1/2}\right)^n\exp\left(-\frac{(R/\ell_\alpha)}{M}\left(\lambda-\Lambda_{n-1/2}\right)\right)\mathrm{d}\lambda\right.$$
$$\left.-\int_{\Lambda_{n+1/2}}^{\infty}\Phi''_{\mathrm{W}}(\lambda)\left(\lambda-\Lambda_{n+1/2}\right)^n\exp\left(-\frac{(R/\ell_\alpha)}{M}\left(\lambda-\Lambda_{n+1/2}\right)\right)\mathrm{d}\lambda\right\},\quad x\to-\infty, \tag{3.27}$$

where

$$\Lambda_\nu = -\left(\frac{U[t]}{R}-\frac{2\nu M\ell}{R}-\frac{\ell_h}{R}\right), \tag{3.28}$$

and Φ''_{W} is the non-dimensional function defined by

$$\Phi''_{\mathrm{W}}(\lambda) = R\frac{\partial^2\varphi^*_\alpha}{\partial x^2}(x,0,0),\quad \text{with } \lambda=\frac{x+\ell_h}{R}, \tag{3.29}$$

which is non-zero only close to the window near $\lambda = (x+\ell_h)/R = 0$ (curve W in figure 2*b*).

The corresponding plots of p_{W} and $\partial p_{\mathrm{W}}/\partial t$ (normalized as in (3.26)) are depicted in figure 3(*b*). The influence of the window first makes itself felt at $U[t]/R \sim 6$; the first peak in the pressure gradient is produced by the first integral in the braces of (3.27) for $n = 0$, $(\nu = -\frac{1}{2})$. Reference to curve W in figure 2(*b*) reveals that $\Phi''_{\mathrm{W}}(\lambda)$ (where $\lambda \equiv (x+\ell_h)/R$) is small when $|\lambda| > 1$, and therefore that the contribution from the first integral is negligible until $\Lambda_{-1/2}$ is smaller than about 1, i.e. until $U[t]/R > 6$. When the nose first interacts with the window (at time $\sim \ell_h/U$) two equal positive pulses are generated, one propagating into the tunnel (the 'peak' near $U[t]/R = 7$ in the figure) and the other propagating to the open end of the hood. Reflection of the latter produces a negative pulse whose transmission into the tunnel (after an overall time delay of $2\ell/c_o$) gives rise to the negative dip in the pressure gradient centred on $U[t]/R = 13$ (where $\Lambda_{1/2} \sim 0$). The second integral in the braces of (3.27) for $n = 0$ is the negative pulse produced by reflection from the open end of the hood; it is partially reflected at the window, however, so that the amplitude of the negative pulse transmitted into the tunnel is reduced by an amount determined by the first integral in the braces for $n = 1$ (whose lower limit of integration is also $\Lambda_{1/2}$). Higher-order terms in the infinite series represent effects of further and multiple reflections of waves within the hood, and make progressively smaller contributions to $\partial p_{\mathrm{W}}/\partial t$, such that the pressure p_{W} rapidly attains its asymptotic value (3.18) (equal non-dimensionally to 0.64) when $U[t]/R > 20$.

The overall non-dimensional pressure p_{SN} of (3.21) and pressure gradient $\partial p_{\mathrm{SN}}/\partial t$ are plotted in figure 3(*c*). It follows from our discussion above that the two large peaks in the pressure gradient respectively at $U[t]/R \sim 0,\ 7$ are the principal effects of the interaction of the nose with the hood portal and with the window. We shall see (§ 4) that the large decrease in pressure between these times (labelled A in the figure) is a consequence of the irrotational approximation, and is countered in practice by a

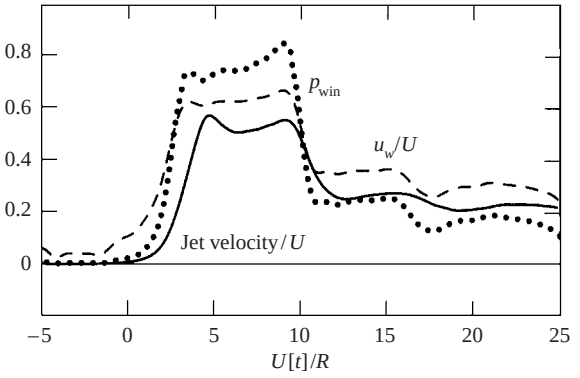

FIGURE 4. The measured hood pressure $p_{\rm win}$ opposite the window normalized as in (3.26) (···) and the measured jet velocity/U (——) for the experimental conditions (4.1)–(4.4); and the steady-state velocity u_w/U (- - - -) calculated from Bernoulli's equation (4.5). $U = 352\ \mathrm{km\,h^{-1}},\ \ell_x = 0.8R,\ \ell_\theta = 0.4R,\ \ell_h = 10R$.

pressure pulse that can be attributed to the vorticity in the shear layer of the jet flow from the window.

4. Influence of the window jet

The increase in pressure in front of the train as it enters the hood produces a high-speed jet flow from the window. The model-scale experiments described in § 5 indicate that the pressure at the window rises rapidly to an approximately uniform value at time $\sim \ell/c_o$ after the train nose enters the hood (roughly equal to the time required for sound to travel from the hood portal to the window); the jet speed also increases to a steady maximum but with a small phase lag. The jet velocity subsequently decreases to about half its maximum value as the nose passes the window because the mean driving pressure is sharply reduced by the acceleration of the air over the nose. This is illustrated by the experimental results shown in figure 4.

In the experiment the interior hood and tunnel radius $R = 5\,\mathrm{cm}$, wall thickness $\ell_w = 0.1R$, the hood length $\ell_h = 10R$, and the model train had an ellipsoidal nose defined by

$$r = h\sqrt{\frac{x}{L}\left(2 - \frac{x}{L}\right)},\ \ 0 < x < L\ \ \ (r = \sqrt{y^2 + z^2}), \tag{4.1}$$

where

$$h = 2.235\,\mathrm{cm}, \quad L = 6.705\,\mathrm{cm}. \tag{4.2}$$

Thus, the blockage $\mathscr{A}_o/\mathscr{A} = 0.2$ and the aspect ratio of the nose $h/L = \frac{1}{3}$. The train had an overall length of 123.9 cm. If s denotes distance measured from the front of the train, then (ignoring the rear end of the train)

$$\frac{\mathscr{A}_{\rm T}(s)}{\mathscr{A}_o} = \begin{cases} s/L\,(2 - s/L), & 0 < s < L, \\ 1, & s > L. \end{cases} \tag{4.3}$$

For the case illustrated in figure 4

$$U = 352\,\mathrm{km\,h^{-1}}, \quad \ell_x = 0.8R, \quad \ell_\theta = 0.4R. \tag{4.4}$$

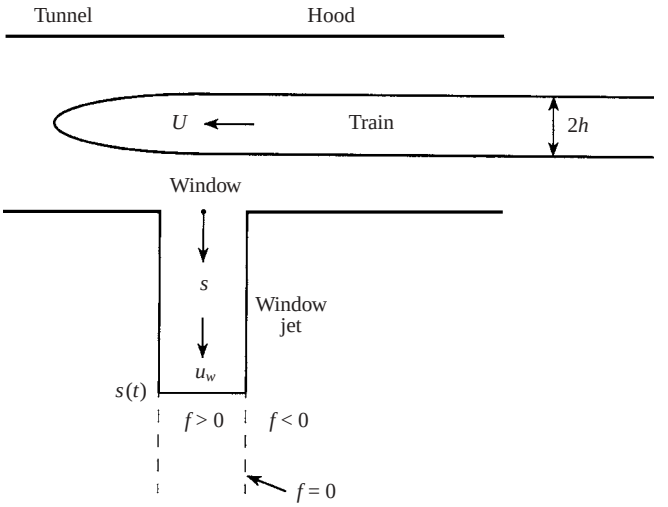

FIGURE 5. Schematic illustration of the model jet flow from the window.

The pressure p_{win}, say, shown normalized as in (3.26) by the dotted curve in figure 4, was measured by means of a sensor placed on the tunnel wall opposite the window. The jet velocity (solid curve) was obtained using a hot wire just outside the centre of the window, and normalized with respect to the train speed U.

Also shown (dashed curve) is the velocity

$$u_w = \sqrt{\frac{2p_{\text{win}}}{\rho_o}} \tag{4.5}$$

given by the time-independent form of Bernoulli's equation. When this formula is applicable it actually determines the maximum jet velocity at the *vena contracta* and just inside the jet shear layer, and therefore exceeds the mean velocity in the plane of the window.

The jet flow from the window occurs principally over a time $\sim O(\ell_h/U)$. To calculate the contribution p_{J}, say, of the jet vorticity to the tunnel pressure wave the jet will be treated as a cylindrical slug of air of increasing length $s(t)$. Figure 5 depicts a schematic representation of this model. It will be seen below that the dominant contribution to the pressure pulse at time t is governed by jet vorticity near the window. Therefore, in a first approximation, it can be assumed that the velocity $\boldsymbol{u}_w(t)$ does not vary with position along the jet, and the contraction of the jet cross-section can be ignored. Let $f(\boldsymbol{x}) = 0$ define the cylindrical boundary of the jet, where $f > 0$ within the jet and $f < 0$ outside. The velocity and vorticity distributions in the jet are then given by

$$\boldsymbol{v} = \boldsymbol{u}_w(t)\mathrm{H}(f), \quad \boldsymbol{\omega} = \operatorname{curl}(\boldsymbol{u}_w(t)\mathrm{H}(f)) \equiv \nabla\mathrm{H}(f) \wedge \boldsymbol{u}_w(t), \tag{4.6}$$

where $\mathrm{H}(f)$ is the Heaviside step function. The vorticity translates at velocity $\frac{1}{2}\boldsymbol{u}_w(t)$, so that in equation (3.3), at distance s along the jet from the window, we can set

$$\boldsymbol{\omega} \wedge \boldsymbol{v} = (\nabla\mathrm{H}(f) \wedge \boldsymbol{u}_w) \wedge \tfrac{1}{2}\boldsymbol{u}_w = -\tfrac{1}{2}u_w^2 \nabla\mathrm{H}(f), \quad 0 < s < s(t). \tag{4.7}$$

The integral containing this term on the right of (3.3) in region B of figure 2 is evaluated using the local representation $G_{\text{W}}(\boldsymbol{x}, \boldsymbol{x}', t-\tau)$ of the Green's function, given by (3.14).

If we temporarily adopt the following shorthand representation of the right-hand side of (3.14):

$$G_{\mathrm{W}}(\boldsymbol{x}, \boldsymbol{x}', t-\tau) = \varphi_\alpha^*(\boldsymbol{x}')\mathscr{F}([t]-\tau), \qquad x \to -\infty, \tag{4.8}$$

then

$$p_{\mathrm{J}} \approx \rho_o \int_{-\infty}^{\infty} \tfrac{1}{2} u_w^2(\tau)\mathscr{F}([t]-\tau)\,\mathrm{d}\tau \int (\nabla H(f)\cdot\nabla\varphi_\alpha^*)(\boldsymbol{x}')\,\mathrm{d}^3\boldsymbol{x}'. \tag{4.9}$$

Now, $\nabla \mathrm{H}(f) \equiv \delta(f)\nabla f$, and the second (volume) integral in this expression is just minus the flux of the potential flow from the window defined by φ_α^* through the cylindrical surface of the jet. This can be evaluated exactly when $s(\tau)$ and φ_α^* are known.

In general it is necessary to determine φ_α^* numerically which, however, cannot be justified unless the jet flow is also determined to the same precision. But it is hardly likely that the dominant characteristics of p_{J} will be critically dependent on the shape of the window. Therefore, for the purpose of this comparison with experiment the flux will be evaluated by replacing φ_α^* by the velocity potential of flow from a circular window of the same area, of radius $R_o = \sqrt{\ell_x \ell_\theta/\pi}$; this can be done analytically (Rayleigh 1926). Then

$$\int (\nabla H(f)\cdot\nabla\varphi_\alpha^*)(\boldsymbol{x}')\,d^3\boldsymbol{x}' = 2\mathscr{A}\{\Psi(s(\tau)) - \Psi(0)\}, \tag{4.10}$$

where Ψ is the non-dimensional form of the Stokes stream function (Lamb 1932) for potential flow from a circular aperture in a plane wall evaluated on the cylindrical surface of the jet:

$$\Psi(s) = \frac{4R_o^2}{\left(\sqrt{s^2+4R_o^2}+s\right)^{3/2}\left[\left(\sqrt{s^2+4R_o^2}+s\right)^{1/2}+\sqrt{2s}\right]}, \tag{4.11}$$

where s is distance measured along the axis of the jet from the plane of the window (see figure 5).

To evaluate the remaining integration with respect to τ in (4.9) it is necessary to specify $u_w(\tau)$ and $s(\tau)$. To do this we consider first the compression wave generated by the train for irrotational flow. The prediction for a snub-nosed train for conditions (4.4) was discussed in § 3. We can use that solution and the convolution formula (3.20) to work out p_0 for the experimental ellipsoidally nosed train of (4.1)–(4.4). The results (normalized as in (3.26)) are shown by the dotted curves in figure 6, where time is measured from the instant that the front of the train nose crosses the entrance plane of the hood. The pressure p_0 in figure 6(a) attains its first maximum near $[t] = t_{\max}$, say. This maximum value is equal to the corresponding measured window pressure p_{win} (figure 4) near $Ut/R \sim U(\ell/c_o)/R \approx 3$.

The magnitude of this maximum pressure is determined by the first interaction with the window of the pressure wave generated by the nose entering the hood portal; this initial small-time behaviour is governed by the irrotational equations of motion. In an ideal fluid a uniform pressure excess cannot be maintained within the tunnel near the window, because air immediately exhausts from the window (forming a radially symmetric source flow) producing a rapid decrease in the pressure that continues until the arrival of the first reflection from the hood portal and/or the train nose begins to interact with the window (both at $U[t]/R \sim 6$ in figure 3). In a real fluid, however, the air streams from the window in a jet whose inertia opposes the pressure fall in the tunnel. Reference to figure 4 reveals that the jet velocity is approximately constant

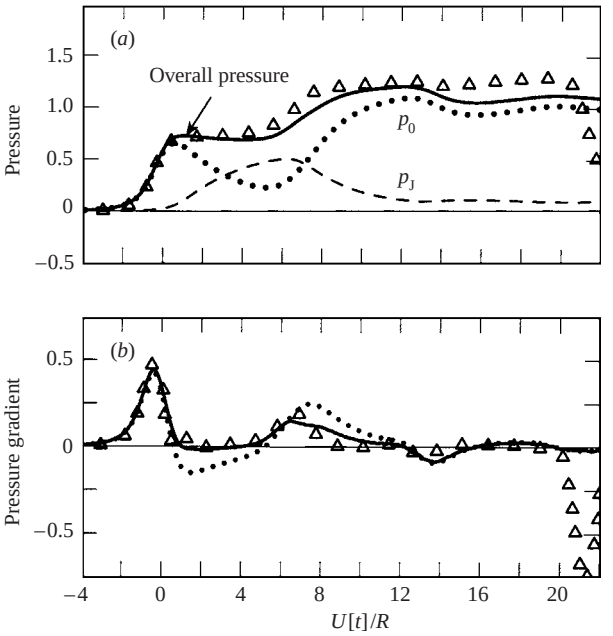

FIGURE 6. Compression wave pressure (a) and pressure gradient (b) normalized as in (3.26) for conditions (4.1), (4.2) and $U = 352\ \mathrm{km\,h^{-1}}$, $\ell_x = 0.8R$, $\ell_\theta = 0.4R$, $\ell_w = 0.1R$: p_0 (···); p_J (- - - -); overall pressure $p_0 + p_J$ (——); the open triangles (△) are the measured pressure and pressure gradient at a distance of 1.5 m from the hood entrance plane.

prior to the arrival of the train nose at the window, which accords with continuity for a train approaching at uniform (low-Mach-number) speed. The kinetic energy of the jet is therefore increasing at a uniform rate, which is possible only if the driving pressure within the tunnel is also approximately constant until the nose reaches the window at $Ut/R \sim 10$. But, this pressure subsequently propagates into the tunnel, forming a uniform component of the compression wave immediately to the rear of the first peak in the compression wave profile, and filling the irrotational trough just behind this maximum (labelled A in figure 3c).

These remarks and the observations of figure 4 lead us to adopt the following approximation in terms of the irrotational pressure p_0 for the principal pressure variations near the window during the passage of the train nose across the hood:

$$p_{\mathrm{win}}(t) \approx \begin{cases} p_0(t - \ell/c_o), & t < t_{\max} + \ell/c_o \\ p_0(t_{\max}), & t_{\max} + \ell/c_o < t < \ell_h/U \\ \frac{1}{4}p_0(t_{\max}), & t > \ell_h/U. \end{cases} \tag{4.12}$$

Figure 4 shows that there is a phase lag δt_J, say, between the attainment of the full jet velocity and the pressure p_{win}. It represents the time required for the arriving pressure wave front to 'fill' the neighbourhood of the window and initiate the jet flow. The value of δt_J is determined by the condition that the predicted pressure must be uniform during the retarded time after the first peak and the arrival of the nose at the window. With this proviso the following modification of the Bernoulli approximation

(4.5) can be used to calculate the jet velocity u_w:

$$u_w(t) = \sqrt{\frac{2p_{\rm win}(t-\delta t_{\rm J})}{\rho_o}}. \tag{4.13}$$

This can be used to evaluate

$$s(t) = \int_{-\infty}^{t} u_w(t')\,{\rm d}t'. \tag{4.14}$$

This formula overestimates the length of the jet at large times, because of the rolling up of the vortex shear layers of the newly formed jet to form a vortex ring. However, for the present window sizes, the function $\Psi(s)$ of (4.11) decays rapidly to zero when s exceeds the tunnel radius R, so that $\Psi(s(\tau))$ in (4.10) is significant only for small values of τ, and rapidly becomes negligible during the significant stages in the development of the window-generated pressure $p_{\rm J}$.

Hence, (4.9) takes the form

$$\begin{aligned} p_{\rm J}(x,t) \approx \frac{(R/\ell_\alpha)}{M}\sum_{n=0}^{\infty}\frac{(R/\ell_\alpha M)^n}{n!}\Bigg\{&\int_{\lambda_{n+1/2}}^{\infty} P_{\rm win}(-\lambda)\{\Psi(S(-\lambda))-\Psi(0)\}\big(\lambda-\lambda_{n+1/2}\big)^n \\ &\times\exp\left(\frac{-(R/\ell_\alpha)}{M}\big(\lambda-\lambda_{n+1/2}\big)\right){\rm d}\lambda - \int_{\lambda_{n-1/2}}^{\infty} P_{\rm win}(-\lambda)\{\Psi(S(-\lambda))-\Psi(0)\} \\ &\times\big(\lambda-\lambda_{n-1/2}\big)^n\exp\left(\frac{-(R/\ell_\alpha)}{M}\big(\lambda-\lambda_{n-1/2}\big)\right){\rm d}\lambda\Bigg\}\quad x\to-\infty, \end{aligned} \tag{4.15}$$

where $\lambda_{n\pm1/2}$ are defined as in (3.23), and

$$S(-\lambda) = s(\tau) \quad\text{and}\quad P_{\rm win}(-\lambda) = p_{\rm win}(\tau-\delta t_{\rm J}) \quad\text{with}\quad \lambda = -\frac{U\tau}{R}. \tag{4.16}$$

This contribution $p_{\rm J}$ to the compression wave pressure is indicated by the dashed curve in figure 6(a) for the experimental conditions (4.1)–(4.4). (The numerical integration in (4.15) was performed after the discontinuity in the definition (4.12) of $p_{\rm win}$ at $t=\ell_h/U$ was removed by assuming the transition to occur smoothly over a time interval $2R/U$.) The solid curve represents the overall predicted pressure $p=p_0+p_{\rm J}$ when the phase lag $U\delta t_{\rm J}/R=1.1$. The maximum of $p_{\rm J}$ is shifted to the left or right in figure 6(a) respectively for smaller or larger values of $\delta t_{\rm J}$, and this choice of $\delta t_{\rm J}$ ensures that p is approximately constant during the retarded time interval between the arrival of the first pressure pulse at the window and the arrival of the train nose. In figure 6(b) we display only the pressure gradients $\partial p_0/\partial t$ and $\partial p/\partial t$ predicted respectively for irrotational flow (dotted curve) and the overall pressure gradient. The jet-generated pressure is seen to fill the pressure trough (labelled A in figure 3c) predicted by the irrotational flow theory before the nose passes the window.

Figure 6 also shows values of the compression wave pressure and pressure gradient (triangles) measured in the tunnel (at a distance of 1 m from the centre of the window). There is reasonable agreement with experiment for all times prior to the arrival of the tail of the train at the hood portal (near $U[t]/R=20$). The discrepancies are significant for $U[t]/R>10$; at such times additional pressure fluctuations produced by flow separation from the train probably account for these differences.

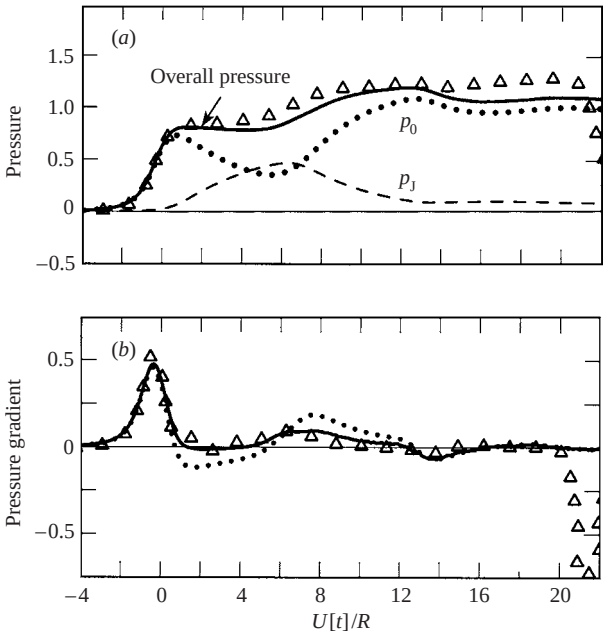

FIGURE 7. Compression wave pressure (a) and pressure gradient (b) normalized as in (3.26) for conditions (4.1), (4.2) and $U = 348$ km h^{-1}, $\ell_x = 0.4R$, $\ell_\theta = 0.4R$, $\ell_w = 0.1R$: p_0 (···); p_J (- - - -); overall pressure $p_0 + p_J$ (——); the open triangles (△) are the measured pressure and pressure gradient at a distance of 1.5 m from the hood entrance plane.

Figure 7 shows a similar comparison with experiment for the same hood with the smaller window, for which

$$U = 348\,\text{km h}^{-1}, \quad \ell_x = 0.4R, \quad \ell_\theta = 0.4R. \tag{4.17}$$

In this case the phase lag $U\delta t_J/R = 1$.

5. Model-scale experiments

5.1. *Experimental apparatus*

Model-scale experiments and flow visualization studies of the window jet were conducted at the Railway Technical Research Institute in Tokyo. Similarity between full-scale and model-scale flows is assured at the same train Mach numbers because the Reynolds number of the dominant air flow induced by a high-speed train is large enough for the initial interactions of the train and tunnel to be regarded as inviscid (Ozawa *et al.* 1976; Ozawa & Maeda 1988*a*). The model-scale experiments reported here are at 1/127 of full scale.

The experimental apparatus is illustrated schematically in figure 8. It is similar to that used by Howe, Iida & Fukuda (2003) to investigate compression wave formation in an unvented hood, which was, in turn, an improved version of one described by Howe *et al.* (2000). The uniform tunnel consists of a 6 m long horizontal circular cylindrical pipe made of hard vinyl chloride, with inner and outer diameters respectively equal to 10 cm and 11.4 cm, fitted with a hood of equal internal diameter and length 50 cm. The axisymmetric model trains were projected into the tunnel by means of a three-stage friction drive involving three pairs of vertically aligned wheels; the train was guided along a 5 mm diameter taut steel wire extending along the tunnel

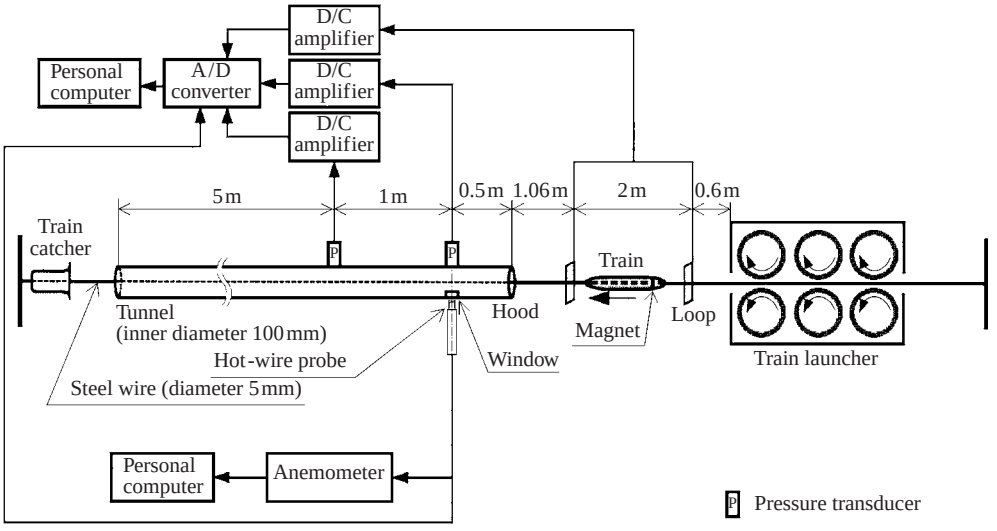

FIGURE 8. Schematic of the experimental apparatus.

axis. The maximum possible launch speed is about 450 km h^{-1}, the actual speed being controlled by varying the rates of rotation of the drive wheels.

A 3.7 m long 'open' section between the launcher and the hood entrance is large enough to ensure that the spherically spreading pressure waves generated during the rapid acceleration of the train are negligible at the hood entrance. On emerging from the far end of the tunnel, the train is brought to rest without damage by a 'catcher' that slides along the steel wire. The overall length (6.5 m) of the tunnel and hood was chosen to ensure that measurements of the compression wave were not affected by wave reflection from the far tunnel exit.

The hood (figure 9*a*) was fabricated from the same size and material cylindrical stock as the tunnel. However, the outer surface of the hood and tunnel were shaved near the window to reduce the outer diameter from the original value of 11.4 cm to 11 cm, thereby achieving a wall thickness at the window of 5 mm (so that $\ell_w = 0.1R$). A rectangular window of azimuthal length 2 cm was located with its centroid 0.5 m from the hood entrance; the axial length of the window was 2 or 4 cm ($\ell_x = 0.4R$ or $0.8R$), and was changed by inserting or removing prefabricated, flush-fitting inserts at both ends of the window. Care was taken to ensure smooth and airtight fits of the inserts and of the join between the tunnel and hood.

The model train (figure 9*b*) was an axisymmetric body with the size and shape specified at the beginning of § 4. It was made from a nylon plastic material of total mass 840 g. The steel guide-wire passes axisymmetrically through a cylindrical hole in the model of diameter 5.5 mm. For these dimensions the blockage $\mathscr{A}_o/\mathscr{A} = 0.2$ (or 0.198 if account is taken of the cross-sectional area of the guide-wire), which is typical of the larger values arising in practice, where for high-speed operations ($U > 200$ km h^{-1}) $\mathscr{A}_o/\mathscr{A}$ is usually restricted to the range 0.12 to 0.22.

5.2. *Measurement procedures*

Small permanent magnets made of neodymium inserted in the model train, and two wire loops placed 2 m apart in the open section between the launcher and the hood entrance were used to measure train speed by detection of the magnetic field of the

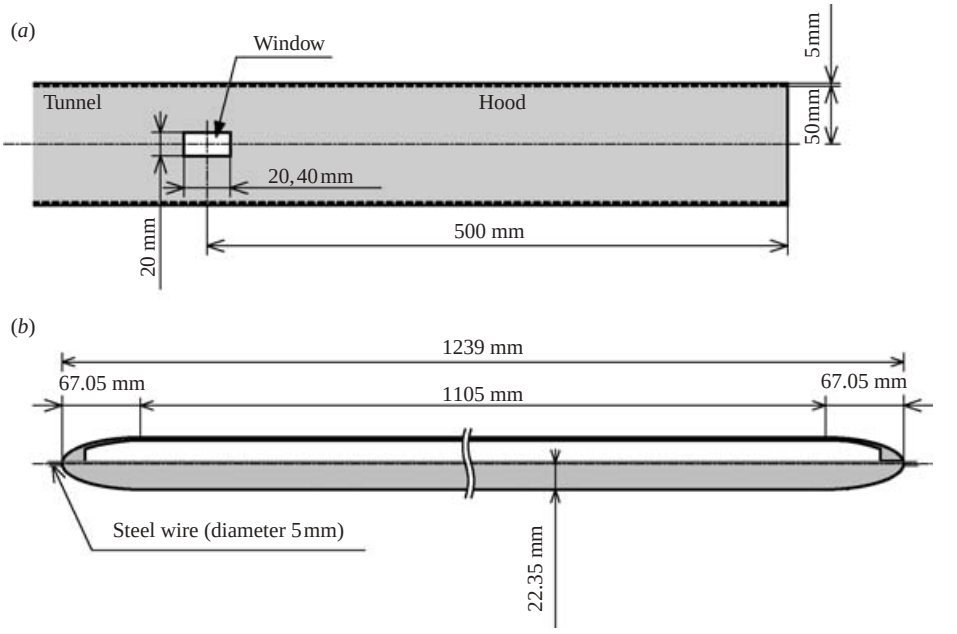

FIGURE 9. (*a*) Scale model entrance hood with a rectangular window. (*b*) Axisymmetric model train with ellipsoidal nose and tail. The steel wire passes through a smooth cylindrical hole along the train axis.

passing train. (The distance between the wire loops was twice that used by Howe *et al.* (2003) to increase the accuracy of the speed measurement.)

The pressure within the tunnel was measured by two *Kulite Semiconductor Products XCS-190-5G* transducers, flush mounted in the tunnel wall at distances of 0.5 m and 1.5 m from the entrance plane of the hood. The first sensor at 0.5 m was diametrically opposite the centroid of the window and was used to measure the 'window pressure' p_{win} of §4 (figure 10). The initial form of the compression wave was measured by the second sensor at 1.5 m. The pressure data were passed through a *TEAC SA-59* amplifier, digitized using a 12-bit analogue-to-digital converter with a sampling rate of 25 kHz per channel, and stored in a personal computer. The pressure gradient $(\mathrm{d}p/\mathrm{d}t)$ was calculated using a simple central difference scheme after high-frequency components (>1 kHz) of the measured pressure were removed using a fast Fourier transform algorithm.

The overall error of the speed measurement is estimated to be no more than about 0.5%. It was also estimated that the tolerance error in the train cross-section is about 1%. Hence, because the compression wave amplitude is proportional to $U^2\mathscr{A}_o/\mathscr{A}$, it can be concluded that the overall errors in measurements of the pressure and pressure gradient are respectively of order 2% and 3%.

The window jet velocity was measured by a *Kanomax IHW-100* constant-temperature anemometer with a *Kanomax 0252R-T5* X-array hot-wire probe (5 μm diameter tungsten wire, frequency response up to 10 kHz). Velocity calibration of the probe was performed by means of a *Kanomax 1065* calibrator for the range of 0–100 m s^{-1}. Velocity data were sampled at the rate of 5 kHz per channel and stored in a personal computer. The hot-wire probe was positioned at the centre of the window as indicated in figure 10. The probe tip was within ± 0.5 mm of the outer radius of

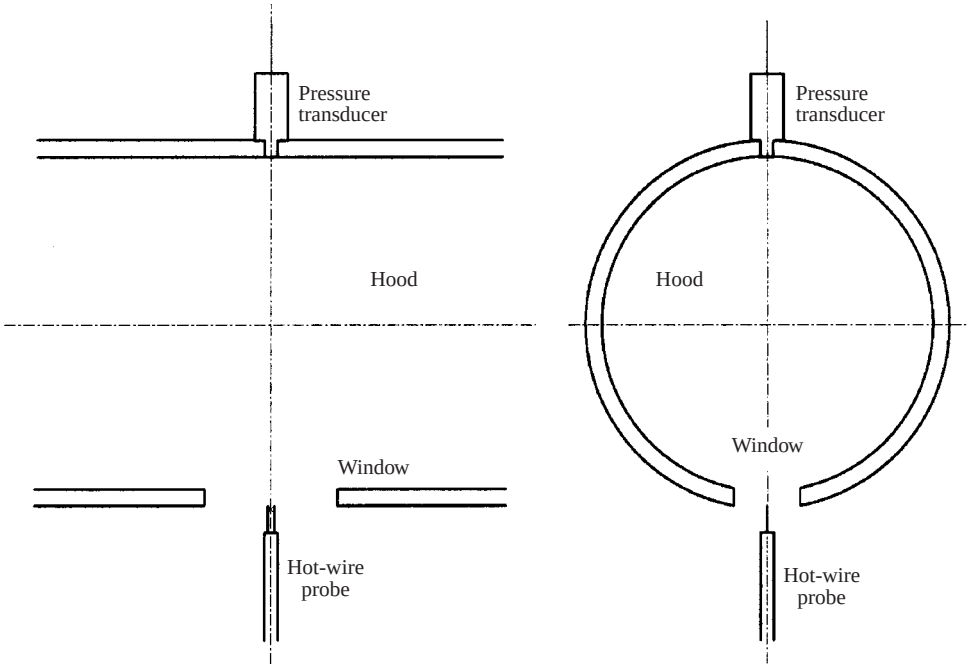

FIGURE 10. Pressure transducer and hot-wire probe for measuring p_{win} and the jet velocity.

the window with the probe axis on the radius from the centre of the cylinder. The two X-array wires were adjusted to be parallel to the (x, z)-plane (see figure 1 for coordinate definition) by rotating the probe about its axis. Because the wires lie in the plane of symmetry $y = 0$, and the velocity in the y-direction can be assumed to vanish, the measured velocity in the direction of the probe axis (the z-direction) supplies the jet velocity at the centre of the window (solid curve in figure 4).

A preliminary experiment was performed to assess the possible influence of the hot-wire probe (of diameter 4 mm) on the window pressure p_{win}. The train was launched into the hood with a $0.4R \times 0.4R$ window at $353\,\text{km}\,\text{h}^{-1}$ in two cases: with and without the hot-wire probe placed at the window. The resulting observations of p_{win} exhibited no discernible differences, and it was therefore concluded that the finite size of the probe did not significantly modify the pressure within the hood and tunnel.

Because pressure and jet velocity were measured by different systems, and because of the importance (see § 4) of the time lag δt_{J} between p_{win} and the jet velocity, it was important that both measurements be referenced to a common time origin. This was done by tapping the hot-wire signal into the pressure measurement system. This permitted the time origins of data stored by each system to be synchronized after data acquisition. The effectiveness of this procedure was confirmed by means of a preliminary experiment in which the acoustic pressure and particle velocity were measured for a plane wave propagating in a tunnel without a window.

5.3. *Flow visualization*

A different hood model made from transparent acrylic resin was used to make simultaneous observations of the model train passing through the hood and the air flow from the window. The transparent hood had the same dimensions as that used to make the pressure and velocity measurements.

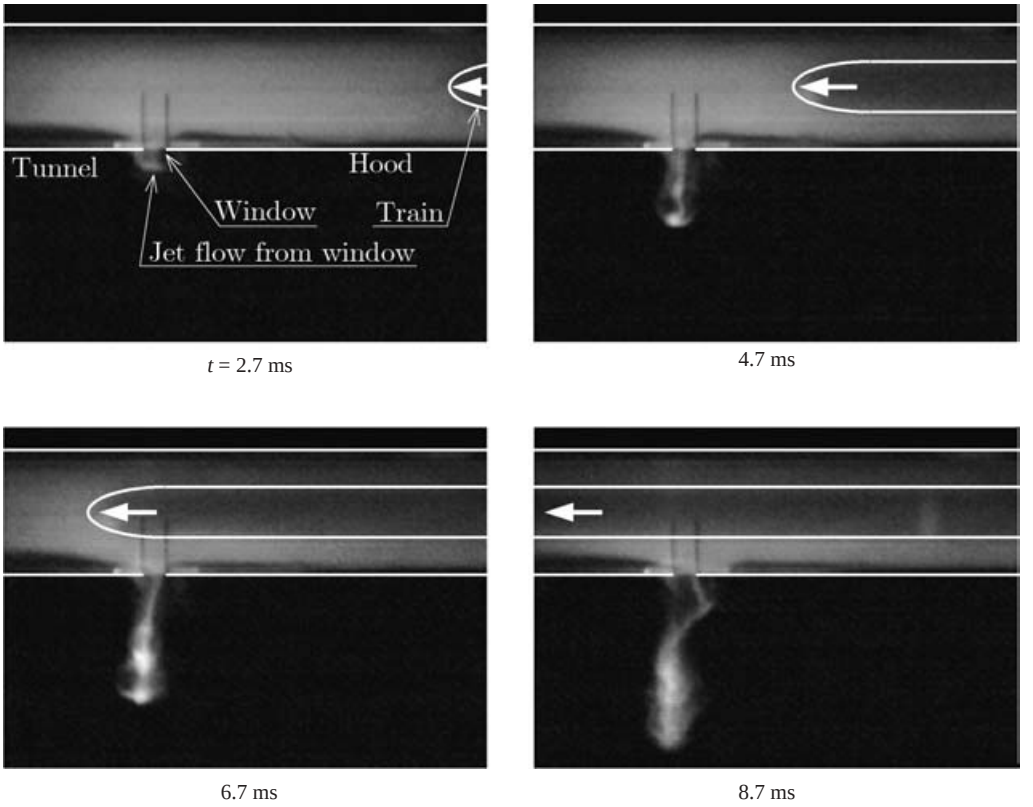

FIGURE 11. Smoke visualizations of the window jet when $U = 299\,\mathrm{km\,h^{-1}}$, $\ell_h = 10R$, $\ell_x = 0.4R$, $\ell_\theta = 0.4R$, $\ell_w = 0.1R$, at times $t = 2.7$, 4.7, 6.7, 8.7 ms after the front of the train nose enters the hood. In the first frame, at $t = 2.7$ ms, the nose is approximately an axial distance $5.5R$ from the centre of the window.

The jet flow was made visible using kerosene smoke. The hood was filled with smoke just prior to launching the train; the air exhausting from the window and the hood portal during train entry was then photographed. (This technique was used by Auvity & Bellenoue (1998) to reveal the back-flow and vortex ring ejected from a tunnel portal by an entering train.) The images were recorded by a high-speed CCD video camera at a rate of 500 frames per second and a shutter speed of 1/10000 s.

Photographs of the flow from the window at the times 2.7, 4.7, 6.7 and 8.7 ms after the entrance of the train nose into the hood are shown in figure 11. The train is advancing from the right at $U = 299\,\mathrm{km\,h^{-1}}$ in the case where $\ell_h = 10R$, $\ell_x = 0.4R$, $\ell_\theta = 0.4R$, $\ell_w = 0.1R$. When the nose enters the hood the pressure in front of the train rises; the pressure rise propagates to the window and air begins to flow from the window ($t = 2.7$ ms, where the nose has reached a distance $5.5R$ from the centre of the window). The outflow emerges as a concentrated jet headed by an approximately rectangular vortex 'ring' formed by the roll-up of the vortex sheets springing from the periphery of the window. As the train nose approaches the window, the high pressure p_{win} at the window is maintained at an approximately constant value (figure 4) and air flows out of the window at a constant volume flux ($t = 4.7$ ms). When the nose passes the window, however, the thinning of the smoke near the root of the jet for

$t = 6.7$ and 8.7 ms indicates that the outflow is reduced because of the rapid decrease in p_{win}. These observations support the theoretical model introduced in § 4.

6. Conclusion

The compression wave generated when a train enters a tunnel with a uniform hood is formed in two stages. The train is acoustically equivalent to a translating distribution of monopole and dipole sources. The interaction of these sources with the hood portal generates first a positive pressure rise which propagates into the hood. This wave is transmitted into the tunnel after interacting with the junction between the hood and tunnel. In this paper we have considered the canonical case in which the hood and tunnel have the same cross-sectional area, and where the junction between the hood and tunnel is marked by the presence of a single rectangular 'window' through which high-pressure air can escape to the atmosphere. A second component of the compression wave is generated when the nose of the train passes the window. Both interactions of the train with the hood portal and the window produce disturbances that are temporarily trapped within the hood by reflections from its ends prior to being radiated into the tunnel. The net effect of these multiple reflections is to produce a 'rippled' profile of the pressure rise across the compression wavefront. However, the overall pressure rise across the wavefront is ultimately the same as if the window were absent.

An open window behaves as a pressure node at very low frequencies, which causes the details of the compression wave profile to be strongly dependent on train Mach number. Air is forced out of the window by the approaching train forming a high-speed jet, and the inertia of this air plays a crucial role in determining the dependence of the wave profile on Mach number. Relatively large oscillations in the pressure are predicted to follow the initial pressure rise if the fluid motion in the window is assumed to be irrotational (so that streamlines of the exiting air flow resemble those of a point source). In the real flow vorticity is generated at the periphery of the window by the passing train, and a jet is formed. The back reaction of the jet on the window produces an additional localized rise in pressure that propagates into the tunnel as a pressure pulse. This pulse 'smooths' the rippled compression wavefront predicted by irrotational theory.

The analytical predictions agree well with our model-scale tests provided proper account is taken of the phase lag δt_{J} between the arrival of the first pressure rise at the window, produced by the interaction of the train nose with the hood portal, and the formation of the jet. The essentially steady and incompressible motion of the air in the tunnel near the window during the time interval between the arrival of the pressure-wave front and the nose of the train implies that the tunnel pressure near the window is temporarily constant, and this condition is used to fix the value of δt_{J}.

It would, no doubt, be possible to obtain full agreement between experiment and predictions based on a numerical treatment of the problem using, say, the compressible Euler equations of motion. However, because of the need to account for the relative motions of the tunnel and train at each time step, the run-time for a complete calculation would be typically several hours, as opposed to the few seconds required for the present method. An entirely numerical approach would also make it difficult to isolate the separate contributions to the overall pressure from the hood portal, the window and the window jet, which is necessary for a proper understanding of compression wave generation and entrance-hood design.

The authors express their gratitude to Dr K. Kikuchi of the Railway Technical Research Institute for supplying the computer code used to evaluate the numerical solutions of Laplace's equation displayed in figure 13, and also to Dr M. Suzuki of the same institute for his assistance with the flow visualization studies.

Appendix. Green's function

A.1. *Statement of the problem*

The solution of the compression wave equation (2.3) is required within the tunnel in $x < -\ell_h$, ahead of the train. The source terms on the right-hand side are significant only during the interval in which the train nose crosses the hood, so that the source point $\boldsymbol{x}'$ of Green's function $G(\boldsymbol{x}, \boldsymbol{x}', t-\tau)$ may be regarded as confined to the vicinity of the hood. To determine G we set

$$G(\boldsymbol{x}, \boldsymbol{x}', t-\tau) = -\frac{1}{2\pi}\int_{-\infty}^{\infty} \bar{G}(\boldsymbol{x}, \boldsymbol{x}', \omega)\, \mathrm{e}^{-\mathrm{i}\omega(t-\tau)}\, \mathrm{d}\omega. \tag{A 1}$$

Then $\bar{G}$ satisfies

$$\left(\nabla^2 + \kappa_o^2\right)\bar{G} = \delta(\boldsymbol{x} - \boldsymbol{x}'), \quad \text{where } \kappa_o = \frac{\omega}{c_o}. \tag{A 2}$$

This equation will be solved by the usual reciprocal theorem method (Rayleigh 1926), according to which $\bar{G}(\boldsymbol{x}, \boldsymbol{x}', \omega) \equiv \bar{G}(\boldsymbol{x}', \boldsymbol{x}, \omega)$ and the point source in (A 2) is regarded as placed at $\boldsymbol{x}$ within the tunnel and the solution is sought as a function of $\boldsymbol{x}'$ in and near the hood. This is especially convenient for the present problem because the characteristic wavelengths of the principal constituents of the compression wave are much larger than the tunnel radius R, and are accordingly plane waves propagating parallel to the tunnel axis. The solution of (A 2) is therefore required only for those sufficiently small values of $\kappa_o R$ (less than about 3.83; see Noble 1958) that propagating disturbances may be regarded as axially propagating plane waves.

In particular, when x is several tunnel diameters from the window within the tunnel, the reciprocal point source at $\boldsymbol{x}$ generates an acoustic disturbance that propagates (as a function of x') towards the hood in the form of the plane wave

$$\bar{G}_{\mathrm{I}} = \frac{\mathrm{e}^{\mathrm{i}\kappa_o(x'-x)}}{2\mathrm{i}\kappa_o \mathscr{A}}. \tag{A 3}$$

When x' is close to the hood the functional form of $\bar{G}(\boldsymbol{x}', \boldsymbol{x}, \omega)$ is then determined by investigating the 'diffraction' of $\bar{G}_{\mathrm{I}}$ by the window and the hood portal.

A.2. *Diffraction by the window*

It is convenient to investigate first the interaction of a plane wave with the window. This will permit a clearer understanding of the more complicated results for the hood derived in § A.5. To fix ideas we consider the idealized problem illustrated in figure 12(*a*), in which a time-harmonic plane wave with velocity potential $\varphi_{\mathrm{I}} = \mathrm{e}^{\mathrm{i}\kappa_o x'}$ is incident on the window from the left. Let us temporarily take the coordinate origin on the cylinder axis at the axial location O of the centroid of the window. The acoustic frequency is assumed to be sufficiently small that $\kappa_o \ell_x \ll 1$, so that the unsteady air flow in the immediate neighbourhood of the window can be regarded as incompressible (as in the method of Lighthill (1978, Chapter 2)). Then, introducing reflection and transmission coefficients $\mathscr{R}_w$, $\mathscr{T}_w$ defined as indicated in figure 12(*a*)

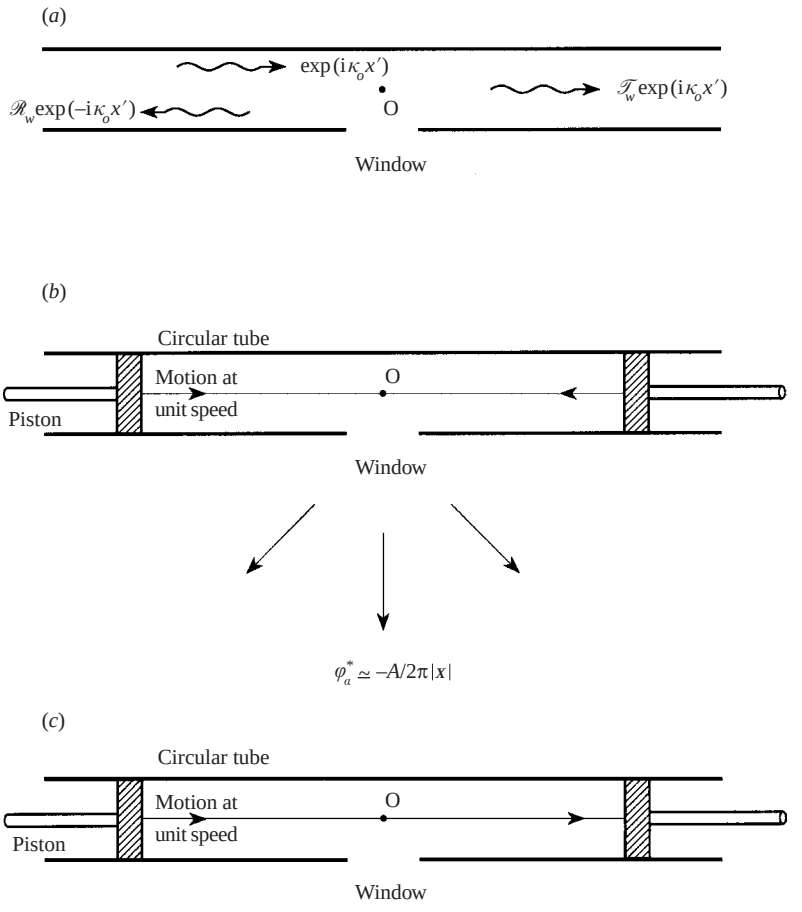

FIGURE 12. (*a*) Potential flow interaction of a plane wave with the window. (*b*) The potential flow problem defining the function φ^*_α. (*c*) The potential flow problem defining the function φ^*_β.

the velocity potential $\varphi(\boldsymbol{x}')$ of the motion can be cast in the forms

$$\varphi = \mathrm{e}^{\mathrm{i}\kappa_o x'} + \mathscr{R}_w \mathrm{e}^{-\mathrm{i}\kappa_o x'} \quad \text{for } x' \text{ far to the left of the window,} \tag{A 4}$$

$$= \alpha_o \varphi^*_\alpha(\boldsymbol{x}') + \beta_o \varphi^*_\beta(\boldsymbol{x}') \text{ in the immediate vicinity of the window,} \tag{A 5}$$

$$= \mathscr{T}_w \mathrm{e}^{\mathrm{i}\kappa_o x'} \text{ far to the right of the window.} \tag{A 6}$$

The functions $\varphi^*_\alpha(\boldsymbol{x}')$, $\varphi^*_\beta(\boldsymbol{x}')$ in (A 5) are solutions of Laplace's equation for the two canonical problems illustrated respectively in figures 12(*b*), 12(*c*): $\varphi^*_\alpha(\boldsymbol{x}')$ is the velocity potential of the incompressible 'monopole' flow out of the window produced by motion of the two pistons towards the window at unit speed. The volume flux through the window is evidently just $2\mathscr{A}$, and a unique specification of $\varphi^*_\alpha(\boldsymbol{x}')$ is obtained by requiring that

$$\varphi^*_\alpha \sim -\frac{\mathscr{A}}{2\pi|\boldsymbol{x}'|}, \quad |\boldsymbol{x}'| \to \infty,$$

where $|\boldsymbol{x}'|$ may be taken to be distance outside the window from the window centroid. Similarly, $\varphi^*_\beta(\boldsymbol{x}')$ represents the 'dipole' flow produced when both pistons move at unit

speed to the right (in the positive x'-direction) with no net flow out of the window, so that

$$\varphi_\beta^* \sim O\left(\frac{1}{|\boldsymbol{x}'|^2}\right), \quad |\boldsymbol{x}'| \to \infty \text{ outside the window.}$$

Equation (A 5) is applicable provided the motion in the neighbourhood of the window can be regarded as locally incompressible; the respective contributions to this motion from the monopole and dipole flows are determined by the magnitudes of the coefficients α_o and β_o.

Within the tunnel, at large distances from the window

$$\left.\begin{aligned} \varphi_\alpha^* &\sim -|x'| - \ell_\alpha, \\ \varphi_\beta^* &\sim x' - \ell_\beta \mathrm{sgn}(x'), \end{aligned}\right\} \; |x'| \gg R, \tag{A 7}$$

where the lengths ℓ_α, ℓ_β depend on the shape and size of the window and on the tunnel radius R. The length ℓ_α is related to the 'conductivity' K of the window (Rayleigh 1926; Howe 1998*a*) by

$$\ell_\alpha = \frac{2\mathscr{A}}{K}. \tag{A 8}$$

According to Rayleigh (1926), $K \sim 2\sqrt{\ell_x \ell_\theta/\pi}$ for a rectangular window of dimensions $\ell_x \times \ell_\theta$ in a thin plane wall. Therefore, for a small window the product $\kappa_o \ell_\alpha$ can be large, even for long-wavelength sound for which $\kappa_o R$ is small. For example,

$$K \approx 0.6R, \quad \ell_\alpha \approx 10R$$

for the dimensions $\ell_x = 0.8R$, $\ell_\theta = 0.4R$ typical of those considered in this paper. On the other hand the 'dipole' length ℓ_β is usually very small. For the rectangular window the approximate formulae given in § A.3 indicate that

$$\ell_\beta \sim \frac{\pi \ell_x^2 \ell_\theta}{32\mathscr{A}} \approx 0.008R \quad \text{for} \quad \ell_x = 0.8R, \; \ell_\theta = 0.4R. \tag{A 9}$$

This means that it is usually permissible to set $\kappa_o \ell_\beta = 0$ when $\kappa_o \ell_\alpha \sim O(1)$.

Equations relating the coefficients α_o, β_o, $\mathscr{R}_w$, $\mathscr{T}_w$ in (A 4)–(A 6) are obtained by matching the different representations of φ where their respective regions of validity overlap. For example, to the left of the window ($x' < 0$) in the region where $\kappa_o|x'| \ll 1$ and $|x'| \gg R$, the representations (A 4) and (A 5) must agree so that, invoking the limiting forms (A 7), we can write

$$1 + \mathscr{R}_w + \mathrm{i}\kappa_o x'(1 - \mathscr{R}_w) \equiv \alpha_o(x' - \ell_a) + \beta_o(x' + \ell_\beta),$$

and therefore

$$\left.\begin{aligned} 1 + \mathscr{R}_w &= -\alpha_o \ell_\alpha + \beta_o \ell_\beta, \\ \mathrm{i}\kappa_o(1 - \mathscr{R}_w) &= \alpha_o + \beta_o. \end{aligned}\right\} \tag{A 10}$$

Similarly, by matching the limiting forms of (A 5) and (A 6) in the region $R \ll x' \ll 1/\kappa_o$ to the right of the window, we find

$$\left.\begin{aligned} \mathscr{T}_w &= -\alpha_o \ell_\alpha - \beta_o \ell_\beta, \\ \mathrm{i}\kappa_o \mathscr{T}_w &= -\alpha_o + \beta_o. \end{aligned}\right\} \tag{A 11}$$

Solving (A 10), (A 11) for the reflection and transmission coefficients:

$$\left.\begin{aligned} \mathscr{R}_w &= 1 - \frac{1}{1+\mathrm{i}\kappa_o\ell_\beta} - \frac{1}{1-\mathrm{i}\kappa_o\ell_\alpha} \approx \frac{-1}{1-\mathrm{i}\kappa_o\ell_\alpha}, \\ \mathscr{T}_w &= \frac{1}{1+\mathrm{i}\kappa_o\ell_\beta} - \frac{1}{1-\mathrm{i}\kappa_o\ell_\alpha} \approx \frac{-\mathrm{i}\kappa_o\ell_\alpha}{1-\mathrm{i}\kappa_o\ell_\alpha}, \end{aligned}\right\} \tag{A 12}$$

where the final approximations on the right of these formulae are appropriate when $\kappa_o\ell_\beta \ll 1$. It is readily verified that both the exact and approximate formulae satisfy

$$|\mathscr{R}_w|^2 + |\mathscr{T}_w|^2 = 1,$$

which states that acoustic energy is conserved between the incident, reflected and transmitted plane waves. This is because we have implicitly neglected the compressibility of the air outside the window, i.e. the propagation of energy into the exterior region has been ignored (such losses are known (Rayleigh 1926) to be of the second order of smallness for long waves).

The frequency dependences of $\mathscr{R}_w$, $\mathscr{T}_w$ have the following interpretations. When the frequency is very small, such that $\kappa_o\ell_\alpha \to 0$, we see that $\mathscr{R}_w \to -1$, $\mathscr{T}_w \to 0$, so that no wave energy can propagate past the window, where the flow varies so slowly that the pressure remains constant and equal to that of the ambient atmosphere (i.e. the velocity potential fluctuations vanish at the window). In the opposite extreme where $\kappa_o\ell_\alpha \gg 1$, however, either because the window is very small, or because the acoustic frequency is large, there is a finite time 'lag' before the pressure in the vicinity of the window relaxes back to atmospheric, and before this occurs $\mathscr{R}_w \sim 0$, $\mathscr{T}_w \sim 1$: most of the wave energy is propagated past the window without change.

A.3. *The functions φ_α^* and φ_β^**

An approximate formula for the behaviour of the 'monopole' potential function $\varphi_\alpha^*(\boldsymbol{x})$ within the tunnel, far from the window (near the tunnel axis) can be found by solving Laplace's equation $\nabla^2\varphi_\alpha^* = 0$ subject to the conditions

$$\left.\begin{aligned} &\varphi_\alpha^* \sim -|x| - \ell_\alpha \quad \text{for } |x| \gg R, \\ &\frac{\partial\varphi_\alpha^*}{\partial r} = \frac{2\mathscr{A}}{\pi\sqrt{(\ell_x/2)^2 - x^2}}\,\frac{\delta(\theta)}{R} \quad \text{for } r = R,\ |x| < \frac{\ell_x}{2}, \end{aligned}\right\} \tag{A 13}$$

where (r, θ, x) are cylindrical polar coordinates defined such that $(z, y) = r(\cos\theta, \sin\theta)$. The second line of (A 13) approximates the window by a line sink of strength $2\mathscr{A}$; this ignores the finite azimuthal width of the window, but takes approximate account of the variation with axial distance x of the flow velocity into the sink (this variation being approximated by that for a 'two-dimensional' window of length ℓ_x, see Lamb 1932). The neglect in this model of the finite azimuthal extent of the window is appropriate because, close to the axis of the tunnel, the potential produced by a line sink depends very weakly on its azimuth, whereas the variation of φ_α^* with x can be expected to depend significantly on the axial extent and velocity distribution in the window.

By this means we find that

$$\varphi_\alpha^*(r, \theta, x) = -|x| - \ell_\alpha - \int_{|x|}^{\infty} \left(1 + \frac{\partial\varphi_\alpha^*}{\partial x'}(r, \theta, x')\right) \mathrm{d}x', \tag{A 14}$$

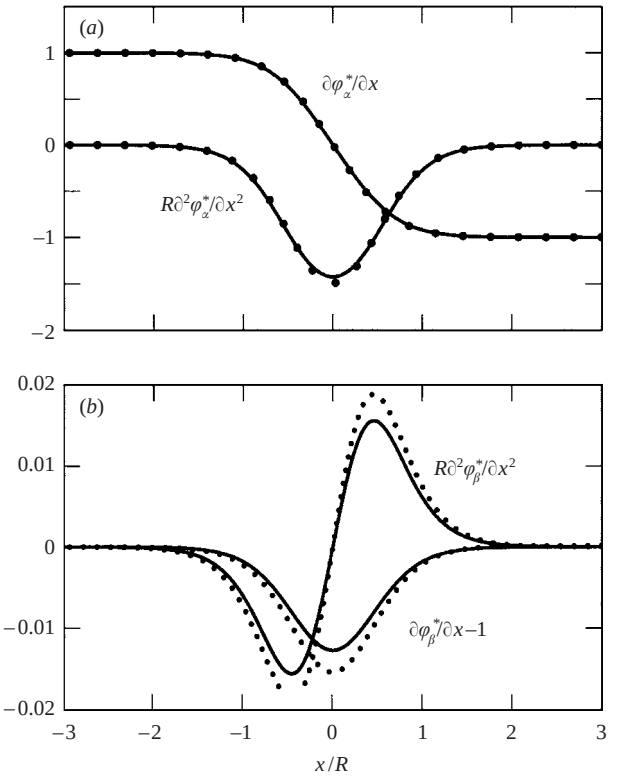

FIGURE 13. Analytical (——) and numerical (···) approximations on the tunnel axis of (*a*) $\partial\varphi_\alpha^*/\partial x$ and $\partial^2\varphi_\alpha^*/\partial x^2$, (*b*) $\partial\varphi_\beta^*/\partial x - 1$ and $\partial^2\varphi_\beta^*/\partial x^2$ for $\ell_x = 0.8R$, $\ell_\theta = 0.4R$.

$$\frac{\partial\varphi_\alpha^*}{\partial x}(r,\theta,x) = -\frac{1}{\pi}\sum_{n=0}^{\infty}\sigma_n\cos n\theta\int_0^\infty \mathrm{I}_n\left(\frac{\lambda r}{R}\right)\mathrm{J}_0\left(\frac{\lambda\ell_x}{2R}\right)\sin\left(\frac{\lambda x}{R}\right)\frac{\mathrm{d}\lambda}{\mathrm{I}_n'(\lambda)}, \tag{A 15}$$

where I_n, J_0 are Bessel functions (Abramowitz & Stegun 1970), the prime on $\mathrm{I}_n'(\lambda)$ denotes differentiation with respect to the argument, and $\sigma_0 = 1$, $\sigma_n = 2$ $(n \geqslant 1)$.

Similarly, the 'dipole' potential function $\varphi_\beta^*(\boldsymbol{x})$ can be approximated near the tunnel axis by the harmonic function satisfying the boundary conditions

$$\left.\begin{aligned} &\varphi_\beta^* \sim x - \ell_\beta\mathrm{sgn}(x) \quad \text{for } |x| \gg R, \\ &\frac{\partial\varphi_\beta^*}{\partial r} = \frac{-x\ell_\theta}{2\sqrt{(\ell_x/2)^2 - x^2}}\,\frac{\delta(\theta)}{R} \quad \text{for } r = R,\ |x| < \frac{\ell_x}{2}, \end{aligned}\right\} \tag{A 16}$$

i.e. by

$$\varphi_\beta^*(r,\theta,x) = x - \frac{\ell_x\ell_\theta R}{8\mathscr{A}}\sum_{n=0}^{\infty}\sigma_n\cos n\theta\int_0^\infty \mathrm{I}_n\left(\frac{\lambda r}{R}\right)\mathrm{J}_1\left(\frac{\lambda\ell_x}{2R}\right)\sin\left(\frac{\lambda x}{R}\right)\frac{\mathrm{d}\lambda}{\lambda\mathrm{I}_n'(\lambda)}. \tag{A 17}$$

The second term on the right of this formula $\sim -\pi\ell_x^2\ell_\theta\mathrm{sgn}(x)/32\mathscr{A}$ for $|x| \gg R$, which yields the approximation for ℓ_β used above in (A 9).

Typical plots (solid curves) of the non-dimensional quantities $\partial\varphi_{\alpha,\beta}^*/\partial x$ and $R\partial^2\varphi_{\alpha,\beta}^*/\partial x^2$ evaluated on the tunnel axis ($r = 0$) using equations (A 15) and (A 17) are depicted in figure 13 for a rectangular window with dimensions $\ell_x = 0.8R$, $\ell_\theta = 0.4R$. The

dotted curves are the corresponding variations obtained by numerical integration of Laplace's equation by the 'boundary element' method (Kikuchi, Maeda & Yanagizawa 1996) for problems (*b*) and (*c*) of figure 12. The component of the compression wave produced by the interaction of the train with the window depends principally on the behaviour of $R\partial^2\varphi^*_{\alpha,\beta}/\partial x^2$ near the window. It is evident from the figure that the relative contribution from the dipole derivative $R\partial^2\varphi^*_{\beta}/\partial x^2$ must be very small.

A.4. *Motion in the hood portal*

The characteristic acoustic wavelength ($\sim R/M$) is large compared to the tunnel and hood radius R. Hence the unsteady motion produced in the neighbourhood of the window W (figure 2) by the reciprocal point source at $\boldsymbol{x}$ can be regarded as irrotational and incompressible, and can therefore be expressed in terms of the potentials φ^*_α and φ^*_β. Similarly, the motion in the mouth of the hood (regions E and A of figure 2) may be regarded as incompressible and represented in terms of the velocity potential $\varphi_{\rm E}(\boldsymbol{x})$, say, that describes irrotational flow from the mouth of a semi-infinite circular cylinder. The formulae for this case are given by Howe (1998*b*) and are quoted here for reference:

$$\left.\begin{aligned}\frac{\partial\varphi^*_{\rm E}}{\partial x}(\boldsymbol{x}) &= \frac{1}{2} - \frac{1}{2\pi}\int_0^\infty \mathrm{I}_0\left(\frac{\xi r}{R}\right)\left(\frac{2\mathrm{K}_1(\xi)}{\mathrm{I}_1(\xi)}\right)^{1/2}\sin\left\{\xi\left(\frac{x}{R}+\mathscr{Z}(\xi)\right)\right\}\mathrm{d}\xi, \quad r<R,\\ \mathscr{Z}(\xi) &= \frac{1}{\pi}\int_0^\infty \ln\left(\frac{\mathrm{K}_1(\mu)\mathrm{I}_1(\mu)}{\mathrm{K}_1(\xi)\mathrm{I}_1(\xi)}\right)\frac{\mathrm{d}\mu}{\mu^2-\xi^2}.\end{aligned}\right\} \tag{A 18}$$

where K_1 is a modified Bessel function, and the coordinate origin is taken at O in the entrance plane of the hood of figure 1. The potential $\varphi^*_{\rm E}$ is normalized such that

$$\begin{aligned}\varphi^*_{\rm E}(\boldsymbol{x}) &\sim x-\ell' \quad \text{when} \quad |x|\gg R \quad \text{in the region H within the hood,}\\ &\sim \frac{-\mathscr{A}}{4\pi|\boldsymbol{x}|} \quad \text{when} \quad |\boldsymbol{x}|\gg R \quad \text{in the region A outside the hood,}\end{aligned} \tag{A 19}$$

where $\ell'\approx 0.61R$ is the 'end-correction' of the hood mouth (Rayleigh 1926).

A.5. *Green's function for a hood of compact diameter*

Turn attention now to the calculation of $\bar{G}(\boldsymbol{x},\boldsymbol{x}',\omega)\equiv\bar{G}(\boldsymbol{x}',\boldsymbol{x},\omega)$, i.e. to the diffraction of the plane wave (A 3) by the hood and window. In the section T of the tunnel (figure 2) to the right of the source ($x'>x$), but at distances $\gg R$ from the window W, the motion consists of that produced by the wave (A 3) together with a reflected wave generated at the window and hood. We therefore write

$$\frac{\bar{G}(\boldsymbol{x}',\boldsymbol{x},\omega)}{\Phi(x,\omega)} = \mathrm{e}^{\mathrm{i}\kappa_o x'} + \mathscr{R}_{\rm T}\mathrm{e}^{-\mathrm{i}\kappa_o x'}, \quad \text{where} \quad \Phi(x,\omega)=\frac{\mathrm{e}^{-\mathrm{i}\kappa_o x}}{2\mathrm{i}\kappa_o\mathscr{A}} \tag{A 20}$$

where $\mathscr{R}_{\rm T}$ is a complex-valued reflection coefficient. We can write down similar representations for $\bar{G}/\Phi$ for positions $\boldsymbol{x}'$ in the neighbourhoods of the points labelled W, H, E, and A in figure 2.

In the mid-section H of the hood the motion will consist of plane waves of the type (A 20) but with different amplitudes. The second-order contribution of compressibility will be neglected outside the hood at A and outside the window at B, so that the motions at E and W can be represented in terms of the potential functions of

§§ A.3, A.4. Hence we set

$$\frac{\bar{G}(\boldsymbol{x}', \boldsymbol{x}, \omega)}{\Phi(x, \omega)} = \alpha\varphi_\alpha^*(\boldsymbol{x}') + \beta\varphi_\beta^*(\boldsymbol{x}') \quad \text{near W}, \tag{A 21}$$

$$= \mathscr{T}_{\mathrm{H}} \mathrm{e}^{\mathrm{i}\kappa_o x'} + \mathscr{R}_{\mathrm{H}} \mathrm{e}^{-\mathrm{i}\kappa_o x'} \quad \text{at H within the hood}, \tag{A 22}$$

$$= \delta\varphi_{\mathrm{E}}^*(\boldsymbol{x}') \quad \text{near E and A}, \tag{A 23}$$

where α, β, $\mathscr{T}_{\mathrm{H}}$, $\mathscr{R}_{\mathrm{H}}$ and δ depend only on the acoustic wavenumber κ_o and the dimensions of the window and hood.

The values of $\mathscr{R}_{\mathrm{T}}$, α, β, $\mathscr{T}_{\mathrm{H}}$, $\mathscr{R}_{\mathrm{H}}$, δ in (A 20)–(A 23) are related by matching the different representations of $\bar{G}/\Phi$ where neighbouring regions of validity overlap. For example, on the left of the window W (centred at $x' = -\ell_h$) where $\kappa_o|x' + \ell_h| \ll 1$ and $|x' + \ell_h| \gg R$, the representations (A 20) and (A 21) must agree, i.e. applying the asymptotic formulae (A 7) (with x' replaced by $x' + \ell_h$ when the coordinate origin is at O in figure 1):

$$\mathrm{e}^{-\mathrm{i}\kappa_o\ell_h} + \mathscr{R}_{\mathrm{T}}\mathrm{e}^{\mathrm{i}\kappa_o\ell_h} + \mathrm{i}\kappa_o(x' + \ell_h)(\mathrm{e}^{-\mathrm{i}\kappa_o\ell_h} - \mathscr{R}_{\mathrm{T}}\mathrm{e}^{\mathrm{i}\kappa_o\ell_h}) \equiv \alpha(x' + \ell_h - \ell_\alpha) + \beta(x' + \ell_h + \ell_\beta),$$

and therefore

$$\left.\begin{aligned} \mathrm{e}^{-\mathrm{i}\kappa_o\ell_h} + \mathscr{R}_{\mathrm{T}}\mathrm{e}^{\mathrm{i}\kappa_o\ell_h} &= -\alpha\ell_\alpha + \beta\ell_\beta, \\ \mathrm{i}\kappa_o(\mathrm{e}^{-\mathrm{i}\kappa_o\ell_h} - \mathscr{R}_{\mathrm{T}}\mathrm{e}^{\mathrm{i}\kappa_o\ell_h}) &= \alpha + \beta. \end{aligned}\right\} \tag{A 24}$$

Similarly, by matching leading-order terms respectively to the right of W and to the left of E in figure 2, we find

$$\left.\begin{aligned} \mathscr{T}_{\mathrm{H}}\mathrm{e}^{-\mathrm{i}\kappa_o\ell_h} + \mathscr{R}_{\mathrm{H}}\mathrm{e}^{\mathrm{i}\kappa_o\ell_h} &= -\alpha\ell_\alpha - \beta\ell_\beta, \\ \mathrm{i}\kappa_o(\mathscr{T}_{\mathrm{H}}\mathrm{e}^{-\mathrm{i}\kappa_o\ell_h} - \mathscr{R}_{\mathrm{H}}\mathrm{e}^{\mathrm{i}\kappa_o\ell_h}) &= -\alpha + \beta. \end{aligned}\right\} \tag{A 25}$$

$$\left.\begin{aligned} \mathscr{T}_{\mathrm{H}} + \mathscr{R}_{\mathrm{H}} &= -\delta\ell', \\ \mathrm{i}\kappa_o(\mathscr{T}_{\mathrm{H}} - \mathscr{R}_{\mathrm{H}}) &= \delta. \end{aligned}\right\} \tag{A 26}$$

Solving the system (A 24–A 26) we find

$$\mathscr{R}_{\mathrm{T}} = -\frac{\mathscr{T}_w(1 + \mathscr{R}_w\mathrm{e}^{2\mathrm{i}\kappa_o\ell})^*\mathrm{e}^{2\mathrm{i}\kappa_o\ell'}}{\mathscr{T}_w^*(1 + \mathscr{R}_w\mathrm{e}^{2\mathrm{i}\kappa_o\ell})}, \tag{A 27}$$

$$\alpha = \frac{2\mathrm{i}\mathscr{T}_w(\sin\kappa_o\ell - \kappa_o\ell_\beta\cos\kappa_o\ell)\mathrm{e}^{\mathrm{i}\kappa_o\ell'}}{(\ell_\alpha + \ell_\beta)(1 + \mathscr{R}_w\mathrm{e}^{2\mathrm{i}\kappa_o\ell})}, \tag{A 28}$$

$$\beta = \frac{2\mathrm{i}\mathscr{T}_w(\sin\kappa_o\ell + \kappa_o\ell_\alpha\cos\kappa_o\ell)\mathrm{e}^{\mathrm{i}\kappa_o\ell'}}{(\ell_\alpha + \ell_\beta)(1 + \mathscr{R}_w\mathrm{e}^{2\mathrm{i}\kappa_o\ell})}, \tag{A 29}$$

$$\mathscr{R}_{\mathrm{H}} = \frac{-\mathscr{T}_w\mathrm{e}^{2\mathrm{i}\kappa_o\ell'}}{1 + \mathscr{R}_w\mathrm{e}^{2\mathrm{i}\kappa_o\ell}}, \tag{A 30}$$

$$\mathscr{T}_{\mathrm{H}} = \frac{\mathscr{T}_w}{1 + \mathscr{R}_w\mathrm{e}^{2\mathrm{i}\kappa_o\ell}}, \tag{A 31}$$

$$\delta = \frac{2\mathrm{i}\kappa_o\mathscr{T}_w\mathrm{e}^{\mathrm{i}\kappa_o\ell'}}{1 + \mathscr{R}_w\mathrm{e}^{2\mathrm{i}\kappa_o\ell}}, \tag{A 32}$$

where $\mathscr{R}_w$ and $\mathscr{T}_w$ are defined as in (A 12), and $\ell = \ell_h + \ell'$.

The formulae (A 28), (A 29) and (A 32) may now be used respectively in (A 21) and (A 23) and then in (A 1) to obtain expressions for $G(\boldsymbol{x}, \boldsymbol{x}', t-\tau)$ that are applicable in the vicinities of the window and hood portal. Since, however, $\partial^2\varphi_\beta^2/\partial x'^2 \ll \partial^2\varphi_\alpha^2/\partial x'^2$, the term involving β will be discarded. This leads to the approximations (3.7) of the main text.

REFERENCES

Abramowitz, M. & Stegun, I. A. (Eds.) 1970 *Handbook of Mathematical Functions* (Ninth corrected printing). US Department of Commerce, National Bureau of Standards Applied Mathematics Series No. 55.

Auvity, B. & Bellenoue, M. 1998 Vortex structure generated by a train tunnel entry near the portal. Paper presented at the *8th Intl Symp. on Flow Visualization, Sorrento, Italy, 1–4 September* (ed. G. M. Carlomagno & I. Grant). Edinburgh University.

Gregoire, R., Rety, J. M., Moriniere, V., Bellenoue, M. & Kageyama, T. 1997 Experimental study (scale 1/70th) and numerical simulations of the generation of pressure waves and micro-pressure waves due to high-speed train-tunnel entry. *Proc. 9th Intl Conf. on Aerodynamics and Ventilation of Vehicle Tunnels, Aosta Valley, Italy, 6–8 October 1997* (ed. J. R. Gillard), pp. 877–902. ME Publications, London.

Hara, T. 1961 Aerodynamic force acting on a high speed train at tunnel entrance. *Q. Rep. Railway Tech. Res. Inst.* **2**(2), 5–11.

Hara, T., Kawaguti, M., Fukuchi, G. & Yamamoto, A. 1968 Aerodynamics of high-speed train. *Mon. Bull. Intl Railway Congr. Assoc.* **XLV**(2), 121–146.

Howe, M. S. 1998*a* *Acoustics of Fluid-Structure Interactions.* Cambridge University Press.

Howe, M. S. 1998*b* The compression wave produced by a high-speed train entering a tunnel. *Proc. R. Soc. Lond.* A **454**, 1523–1534.

Howe, M. S., Iida, M. & Fukuda, T. 2003 Influence of an unvented tunnel entrance hood on the compression wave generated by a high-speed train. *J. Fluids Struct.* **17**, 833–853.

Howe, M. S., Iida, M., Fukuda, T. & Maeda, T. 2000 Theoretical and experimental investigation of the compression wave generated by a train entering a tunnel with a flared portal. *J. Fluid Mech.* **425**, 111–132.

Iida, M., Matsumura, T., Nakatani, K., Fukuda, T. & Maeda, T. 1996 Optimum nose shape for reducing tunnel sonic boom. *Inst. Mech. Engrs Paper* C514/015/96.

Ito, M. 2000 Improvement to the aerodynamic characteristics of Shinkansen rolling stock. *Proc. Inst. Mech. Engrs*: F *J. Rail Rapid Transit* **214**, 135–143.

Kikuchi, K., Maeda, T. & Yanagizawa, M. 1996 Numerical simulation of the phenomena due to the passing-by of two bodies using the unsteady boundary element method. *Intl J. Numer. Meth. Fluids* **23**, 445 –454.

Lamb, H. 1932 *Hydrodynamics*, 6th. Edn. Cambridge University Press (Reprinted 1993).

Lighthill, J. 1978 *Waves in Fluids.* Cambridge University Press.

Maeda, T., Matsumura, T., Iida, M., Nakatani, K. & Uchida, K. 1993 Effect of shape of train nose on compression wave generated by train entering tunnel. *Proc. Intl Conf. on Speedup Technology for Railway and Maglev Vehicles, Yokohama, Japan, 22–26 November, 1993* (ed. M. Iguchi), pp. 315–319. JSME.

Matsuo, K., Aoki, T., Mashimo, S. & Nakatsu, E. 1997 Entry compression wave generated by a high-speed train entering a tunnel. *Proc. 9th Intl Conf. on Aerodynamics and Ventilation of Vehicle Tunnels, Aosta Valley, Italy, 6–8 October 1997*, pp. 925–934. ME Publications, London.

Noble, B. 1958 *Methods based on the Wiener-Hopf Technique.* Pergamon. (Reprinted 1988 by Chelsea Publishing Company, New York.)

Noguchi, Y., Okamura, Y., Uchida, K., Ishihara, T., Mashimo, S. & Kageyama, M. 1996 Solving aerodynamic environmental problems arising from train speed-up. *Inst. Mech. Engrs Paper* C514/039/96.

Ogawa, T. & Fujii, K. 1994 Numerical simulation of compressible flows induced by a train moving into a tunnel. *Comput. Fluid Dyn. J.* **3**, 63–82.

Ogawa, T. & Fujii, K. 1997 Numerical investigation of three dimensional compressible flows induced by a train moving into a tunnel. *J. Computers Fluids* **26**, 565–585.

Ozawa, S. & Maeda, T. 1988*a* Model experiment on reduction of micro-pressure wave radiated from tunnel exit. *Proc. Intl Symp. on Scale Modeling, Japan Society of Mechanical Engineers, Tokyo, 18–22 July* (ed. R. I. Emori).

Ozawa, S. & Maeda, T. 1988*b* Tunnel entrance hoods for reduction of micro-pressure wave. *Q. Rep. Railway Tech. Res. Inst.* **29**(3), 134–139.

Ozawa, S., Maeda, T., Matsumura, T., Uchida, K., Kajiyama, H. & Tanemoto, K. 1991 Countermeasures to reduce micro-pressure waves radiating from exits of Shinkansen tunnels. In *Aerodynamics and Ventilation of Vehicle Tunnels*, pp. 253–266. Elsevier.

Ozawa, S., Morito, Y., Maeda, T. & Kinosita, M. 1976 Investigation of the pressure wave radiated from a tunnel exit. *Railway Tech. Res. Inst. Rep.* 1023 (in Japanese).

Ozawa, S., Uchida, T. & Maeda, T. 1978 Reduction of micro-pressure wave radiated from tunnel exit by hood at tunnel entrance. *Q. Rep. Railway Tech. Res. Inst.* **19**(2), 77–83.

Peters, J. L. 2000 Tunnel optimized train nose shape. Paper presented at the *10th Intl Symp. on Aerodynamics and Ventilation of Vehicle Tunnels, Boston, USA, 1–3 November* (ed. A. S. Caserta). BHR Group.

Rayleigh, Lord 1926 *The Theory of Sound*, vol. 2, chap. XVI. Macmillan (Reprinted 1945, Dover.)

Woods, W. A. & Pope, C. W. 1976 Secondary aerodynamic effects in rail tunnels during vehicle entry. *Second BHRA Symp. on the Aerodynamics and Ventilation of Vehicle Tunnels, Cambridge, UK, 23–25 March 1976*, Paper C5, pp. 71–86 (ed. H. S. Stephens, R. Rosemary Dowden, A. L. King & M. P. Patel). BHRA Fluid Engineering.